

# The Extended Bose-Hubbard Model

---

**Andrea Kouta Dagnino<sup>‡</sup>**

<sup>‡</sup>*Open University, Milton Keynes, UK.*

E-mail: [k.y.dagnino@gmail.com](mailto:k.y.dagnino@gmail.com)

**Supervised by Dr Andrew J.A. James and Dr James P. Hague**

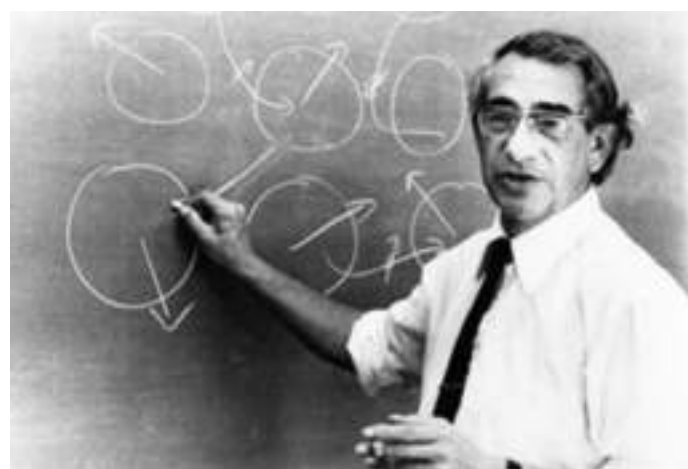
---

# Contents

1	<i>An introduction to Second Quantization</i>	<b>3</b>
1.1	The need for second quantization .	<b>3</b>
1.2	The occupation representation and Fock spaces . . . . .	<b>4</b>
1.3	Creation and annihilation operators	<b>6</b>
1.4	Field operators . . . . .	<b>10</b>
1.5	Quantising the electromagnetic field	<b>15</b>
2	<i>Deriving the Hubbard models</i>	<b>19</b>
2.1	Introduction . . . . .	<b>19</b>
2.2	Derivation for Fermions . . . . .	<b>20</b>
2.3	Derivation for bosons . . . . .	<b>22</b>
2.4	Symmetries of the models . . . . .	<b>24</b>
2.4.1	Translational symmetry . .	<b>24</b>
2.4.2	Parity operator . . . . .	<b>25</b>
2.5	Exact block-diagonalisation results	<b>26</b>
3	<i>The Eigenstate Thermalization Hypothesis (ETH)</i>	<b>27</b>
3.1	Introduction . . . . .	<b>27</b>
3.2	Quantum Ensembles . . . . .	<b>28</b>
3.3	Thermalization in Quantum systems . . . . .	<b>28</b>
3.4	The Eigenstate Thermalization Hypothesis . . . . .	<b>29</b>
3.5	Important remarks on ETH . . . . .	<b>31</b>
3.6	The Quintessential chaotic Bose-Hubbard model . . . . .	<b>33</b>
3.7	Ergodicity breaking: a general overview . . . . .	<b>33</b>
3.8	One-chain model . . . . .	<b>34</b>
3.8.1	The model . . . . .	<b>34</b>
3.8.2	Absence of integrability . .	<b>34</b>
3.8.3	Eigenstate expectation value (EEV) plots . . . . .	<b>37</b>
3.8.4	Off-diagonal matrix elements . . . . .	<b>39</b>
3.8.5	Time evolution and Quenches . . . . .	<b>40</b>
3.9	Two-chain model . . . . .	<b>43</b>
3.9.1	The model and symmetries	<b>43</b>
3.9.2	Energy and EEV spacing statistics . . . . .	<b>43</b>
3.9.3	EEV plots . . . . .	<b>44</b>
3.9.4	Response to Quenches . . .	<b>46</b>
3.10	Conclusions . . . . .	<b>46</b>
	<i>Bibliography</i>	<b>50</b>

---

*John Hubbard (1931-1980)*



# CHAPTER 1

---

## An introduction to Second Quantization

### 1.1 The need for second quantization

Suppose we have an  $N$ -particle system, where particle  $i$  resides in a hilbert space  $\mathcal{H}_i$ . The system as a whole will then be described by a state in the tensor product space  $\bigotimes_{i=1}^n \mathcal{H}_i$ . In the special case where the  $N$ -particles are indistinguishable, special care must be made due to the distinction between fermions and bosons. The states describing bosons will be totally symmetric under particle exchange, and thus belong to the subspace  $\text{Sym}^N \mathcal{H}$  while states describing fermions will be totally anti-symmetric, and belong to the subspace  $\Lambda^N \mathcal{H}$ .

Let  $|\psi\rangle = |\psi^{(1)}\rangle_1 \otimes |\psi^{(2)}\rangle_2 \otimes \dots |\psi^{(N)}\rangle_N \in \mathcal{H}^N$ . This doesn't automatically qualify  $|\psi\rangle$  as a physical state describing bosonic or fermionic systems. We must find a way to symmetrize or anti-symmetrize this state. It can be shown that this can be done through the projection operators:

$$\hat{S}_+ = \frac{1}{\sqrt{N!}} \sum_{\sigma \in S_N} \hat{P}_\sigma \quad (1.1.1)$$

$$\hat{S}_- = \frac{1}{\sqrt{N!}} \sum_{\sigma \in S_N} \text{sgn}(\sigma) \hat{P}_\sigma \quad (1.1.2)$$

known as the symmetrization and anti-symmetrization operators. Using the definition of permanents (denoted by a + sign at the top) and determinants, it follows that:

$$|\psi\rangle_+ = \hat{S}_+ |\psi\rangle = \frac{1}{\sqrt{N!}} \begin{vmatrix} |\psi^{(1)}\rangle_1 & |\psi^{(1)}\rangle_2 & |\psi^{(1)}\rangle_3 & \dots & |\psi^{(1)}\rangle_N \\ |\psi^{(2)}\rangle_1 & |\psi^{(2)}\rangle_2 & |\psi^{(2)}\rangle_3 & \dots & |\psi^{(2)}\rangle_N \\ |\psi^{(3)}\rangle_1 & |\psi^{(3)}\rangle_2 & |\psi^{(3)}\rangle_3 & \dots & |\psi^{(3)}\rangle_N \\ \vdots & \vdots & \vdots & \ddots & \vdots \\ |\psi^{(N)}\rangle_1 & |\psi^{(N)}\rangle_2 & |\psi^{(N)}\rangle_3 & \dots & |\psi^{(N)}\rangle_N \end{vmatrix}^+ \quad (1.1.3)$$

and similarly:

$$|\psi\rangle_- = \hat{S}_- |\psi\rangle = \frac{1}{\sqrt{N!}} \begin{vmatrix} |\psi^{(1)}\rangle_1 & |\psi^{(1)}\rangle_2 & |\psi^{(1)}\rangle_3 & \dots & |\psi^{(1)}\rangle_N \\ |\psi^{(2)}\rangle_1 & |\psi^{(2)}\rangle_2 & |\psi^{(2)}\rangle_3 & \dots & |\psi^{(2)}\rangle_N \\ |\psi^{(3)}\rangle_1 & |\psi^{(3)}\rangle_2 & |\psi^{(3)}\rangle_3 & \dots & |\psi^{(3)}\rangle_N \\ \vdots & \vdots & \vdots & \ddots & \vdots \\ |\psi^{(N)}\rangle_1 & |\psi^{(N)}\rangle_2 & |\psi^{(N)}\rangle_3 & \dots & |\psi^{(N)}\rangle_N \end{vmatrix} \quad (1.1.4)$$

We can write these results more intuitively as:

$$|\psi\rangle_+ = \frac{1}{\sqrt{N!}} (|\psi\rangle + \text{permutations of } |\psi\rangle) \quad (1.1.5)$$

$$|\psi\rangle_- = \frac{1}{\sqrt{N!}} (|\psi\rangle \pm \text{permutations of } |\psi\rangle) \quad (1.1.6)$$

To summarize, we started with some ket where a list of  $N$  states in  $\mathcal{H}$  were occupied by a particle, and produced a new state where each state is still occupied, but that is now (anti-)invariant under any particle exchange. We have gone from thinking about the state of each particle to thinking about which states are occupied.

It is clear that calculations involving permanents and determinants can get very messy in the thermodynamic limit, due to the  $\sim o(N!)$  complexity of evaluating determinants and permanents. A new convention is thus needed to deal with many-body systems such as the ones encountered in condensed matter systems.

The situation is further worsened by a redundancy in the standard notation we have used thus far. Consider the following states:

$$|\Psi_1\rangle = |\psi^{(1)}\rangle_1 \otimes |\psi^{(2)}\rangle_2 \otimes |\psi^{(3)}\rangle_3 \otimes |\psi^{(4)}\rangle_4 \quad (1.1.7)$$

$$|\Psi_2\rangle = |\psi^{(4)}\rangle_1 \otimes |\psi^{(2)}\rangle_2 \otimes |\psi^{(1)}\rangle_3 \otimes |\psi^{(3)}\rangle_4 \quad (1.1.8)$$

$$(1.1.9)$$

It is clear that (anti)-symmetrizing  $|\Psi_1\rangle$  and  $|\Psi_2\rangle$  will give the same state. More generally, for fermionic systems, given any state in  $\mathcal{H}^N$ , there will be  $N!$  states generated by the symmetric group  $S_N$  which get symmetrized to the same state in  $\bigwedge^N \mathcal{H}$ . <sup>1</sup> In other words, the dimension of  $\mathcal{H}^N$  does not match the dimensions of  $\text{Sym}_N \mathcal{H}$  and  $\bigwedge^N \mathcal{H}$ .

## 1.2 The occupation representation and Fock spaces

One important concept that came up in the previous section was the occupation of states. Indeed, in both the symmetrized and anti-symmetrized states, the occupation of each state was preserved. This suggests using a notation where instead of referring which particle occupies which state, we refer to which states are occupied. This is known as the **occupation representation**.

Generally, if we let  $\{|\psi^{(1)}\rangle, |\psi^{(2)}\rangle, \dots, |\psi^{(k)}\rangle, \dots\}$  be an ordered basis of  $\mathcal{H}$ , then we define

$$|n_1, n_2, \dots, n_k, \dots\rangle \quad (1.2.1)$$

---

<sup>1</sup>the situation is more intricate for bosons where a state may be occupied by more than one particle

to be the state where  $|\psi^{(1)}\rangle$  is occupied by  $n_1$  particles,  $|\psi^{(2)}\rangle$  by  $n_2$  particles, etc...

In other words, for bosons we have that:

$$|n_1, n_2, \dots, n_k, \dots\rangle = \sqrt{\frac{N!}{n_1! n_2! \dots n_k! \dots}} \hat{S}_+ \left( \bigotimes_{i=1}^{n_1} |\psi^{(1)}\rangle_i \right) \otimes \left( \bigotimes_{i=1}^{n_2} |\psi^{(2)}\rangle_{n_1+i} \right) \dots \left( \bigotimes_{i=1}^{n_k} |\psi^{(k)}\rangle_{\dots} \right) \dots \quad (1.2.2)$$

where  $N = \sum_i n_i$ , while for fermions:

$$|n_1, n_2, \dots, n_k, \dots\rangle = \sqrt{N!} \hat{S}_- \left( \bigotimes_{i=1}^{n_1} |\psi^{(1)}\rangle_i \right) \otimes \left( \bigotimes_{i=1}^{n_2} |\psi^{(2)}\rangle_{n_1+i} \right) \dots \left( \bigotimes_{i=1}^{n_k} |\psi^{(k)}\rangle_{\dots} \right) \dots \quad (1.2.3)$$

where  $n_i = 0, 1$  by the Pauli exclusion principle. The occupation representation is much more abstract and harder to use for fermions due to their state's anti-symmetry. Indeed, note that:

$$\begin{aligned} |..., n_i = 1, \dots, n_j = 1, \dots\rangle &= \sqrt{N!} \hat{S}_- (\dots \otimes |\psi^{(i)}\rangle \otimes \dots \otimes |\psi^{(j)}\rangle \dots) \\ \implies |..., n_j = 1, \dots, n_i = 1, \dots\rangle &= \sqrt{N!} \hat{S}_- (\dots \otimes |\psi^{(j)}\rangle \otimes \dots \otimes |\psi^{(i)}\rangle \dots) \\ &= - |..., n_i = 1, \dots, n_j = 1, \dots\rangle \end{aligned}$$

Clearly, the order in which we state the occupation of states is important, even though we're still denoting the same physical state.

States in the occupation representation constructed from a single-particle space  $\mathcal{H}$  belong to the combined space of all possible states for an  $N$ -particle system, which we denote as  $\mathcal{F}_N$ :

$$\mathcal{F}_N = \text{Span}\{|n_1, n_2, \dots, \rangle : \sum_i n_i = N\} \quad (1.2.4)$$

For example, letting  $N = 2$  and  $\mathcal{H} = \{|\uparrow\rangle, |\downarrow\rangle\}$  then:

$$\mathcal{F}_2 = \underbrace{\left\{ |\uparrow\rangle_1 \otimes |\uparrow\rangle_2, |\downarrow\rangle_1 \otimes |\downarrow\rangle_2, \frac{1}{\sqrt{2}}(|\uparrow\rangle_1 \otimes |\downarrow\rangle_2 + |\downarrow\rangle_1 \otimes |\uparrow\rangle_1), \right.}_{\in \text{Sym}_2 \mathcal{H}}$$

$$\left. \frac{1}{\sqrt{2}}(|\uparrow\rangle_1 \otimes |\downarrow\rangle_2 - |\downarrow\rangle_1 \otimes |\uparrow\rangle_1) \right\} \quad (1.2.6)$$

The **Fock space**  $\mathcal{F}$  is defined as the direct sum of all  $\mathcal{F}_i$ :

$$\mathcal{F} = \bigoplus_{i=0}^n \mathcal{F}_i \quad (1.2.7)$$

### 1.3 Creation and annihilation operators

#### Bosonic operators

There are two important maps between  $\mathcal{F}_N$  and  $\mathcal{F}_{N+1}$ , known as the creation and annihilation operators. The **bosonic creation operator** is defined as:

$$a_i^\dagger : \mathcal{F}_N \rightarrow \mathcal{F}_{N+1} \quad (1.3.1)$$

$$|n_1, \dots, n_i, \dots\rangle \mapsto \sqrt{n_i + 1} |n_1, \dots, n_i + 1, \dots\rangle \quad (1.3.2)$$

so that (restricting the fock state to the occupation of  $|\psi^{(i)}\rangle$  only):

$$\langle n_i + 1 | a_i^\dagger | n_i \rangle = \sqrt{n_i + 1} \quad (1.3.3)$$

$$\iff \langle n_i | a_i | n_i + 1 \rangle = \langle n_i + 1 | a_i^\dagger | n_i \rangle^* = \sqrt{n_i + 1} \quad (1.3.4)$$

$$\iff a_i |n_i + 1\rangle = \sqrt{n_i + 1} |n_i\rangle \quad (1.3.5)$$

In other words, we have that the hermitian conjugate of the creation operator, known as the **bosonic annihilation operator**, is defined as:

$$a_i : \mathcal{F}_{N+1} \rightarrow \mathcal{F}_N \quad (1.3.6)$$

$$|n_1, \dots, n_i + 1, \dots\rangle \mapsto \sqrt{n_i + 1} |n_1, \dots, n_i, \dots\rangle \quad (1.3.7)$$

These operators allow us to create or destroy particles in a specific state. One must be wary however, since destroying too many particles eventually leads to the destruction of the vacuum state  $|0\rangle$ , where each state is not occupied, giving zero as a result.

We find that if  $i \neq j$ :

$$a_i a_j^\dagger |n_i, n_j\rangle = \sqrt{n_j + 1} \sqrt{n_i} |n_i - 1, n_j + 1\rangle \quad (1.3.8)$$

$$a_j^\dagger a_i |n_i, n_j\rangle = \sqrt{n_i} \sqrt{n_j + 1} |n_i - 1, n_j + 1\rangle \quad (1.3.9)$$

$$\iff [a_i, a_j^\dagger] = 0, \quad i \neq j \quad (1.3.10)$$

while if  $i = j$ :

$$a_i a_i^\dagger |n_i\rangle = \sqrt{n_i + 1} \sqrt{n_i} |n_i\rangle \quad (1.3.11)$$

$$a_i^\dagger a_i |n_i\rangle = \sqrt{n_i} \sqrt{n_i} |n_i\rangle \quad (1.3.12)$$

$$\iff [a_i, a_i^\dagger] = 1 \quad (1.3.13)$$

implying that:

$$[a_i, a_j^\dagger] = \delta_{ij} \quad (1.3.14)$$

Similarly, one finds that:

$$a_i^\dagger a_j^\dagger |n_i, n_j\rangle = \sqrt{n_j + 1} \sqrt{n_i + 1} |n_i + 1, n_j + 1\rangle \quad (1.3.15)$$

$$a_j^\dagger a_i^\dagger |n_i, n_j\rangle = \sqrt{n_i + 1} \sqrt{n_j + 1} |n_i + 1, n_j + 1\rangle \quad (1.3.16)$$

$$\iff [a_i^\dagger, a_j^\dagger] = 0, \quad i \neq j \quad (1.3.17)$$

and since  $[a_i^\dagger, a_i^\dagger] = 0$ , we find that:

$$[a_i^\dagger, a_j^\dagger] = 0 \quad (1.3.18)$$

Therefore:

$$[a_i^\dagger, a_j^\dagger]^\dagger = [a_j, a_i] = 0 \quad (1.3.19)$$

giving:

$$[a_i, a_j] = 0 \quad (1.3.20)$$

These relations define the commutator algebra for bosonic creation/annihilation operators. Moreover, we may also use these operators to generate the Fock space from the vacuum state  $|0\rangle$ , since:

$$|n_1, n_2, \dots, n_i, \dots\rangle = \frac{1}{\sqrt{n_1! n_2! \dots n_i! \dots}} \prod_{i=1}^N (a_i^\dagger)^{n_i} |0\rangle \quad (1.3.21)$$

Finally, (1.3.12) suggests that we define a new operator, the **occupation number operator**  $\hat{n}_i$ , as the following automorphism:

$$\hat{n}_i : \mathcal{F}_N \rightarrow \mathcal{F}_N \quad (1.3.22)$$

$$|n_1, \dots, n_i, \dots\rangle \mapsto n_i |n_1, \dots, n_i, \dots\rangle \quad (1.3.23)$$

which gives the occupation number of the  $i$ th state.

### Fermionic operators

Just as in the case of bose statistics, we may define creation and annihilation operators for fermi statistics. However, care must be taken due to the exchange anti-symmetry of fermions, and a necessary revision to the bosonic operator definition will therefore be required.

The **fermionic creation operator** is defined as:

$$c_i^\dagger : \mathcal{F}_N \rightarrow \mathcal{F}_{N+1} \quad (1.3.24)$$

$$|n_1, \dots, n_i, \dots\rangle \mapsto (-1)^{s_i} \sqrt{n_i + 1} |n_1, \dots, n_i + 1, \dots\rangle \quad (1.3.25)$$

where  $s_i = \sum_{k=1}^{n_i-1} n_k$ .

Consequently, we see that (restricting the fock state to the occupation of  $|\psi^{(i)}\rangle$  only):

$$\langle n_i + 1 | c_i^\dagger | n_i \rangle = (-1)^{s_i} \quad (1.3.26)$$

$$\iff \langle n_i | a_i | n_i + 1 \rangle = \langle n_i + 1 | c_i^\dagger | n_i \rangle^* = (-1)^{s_i} \quad (1.3.27)$$

$$\iff c_i |n_i + 1\rangle = (-1)^{s_i} |n_i\rangle \quad (1.3.28)$$

In other words, we have that the hermitian conjugate of the creation operator, known as the **fermionic annihilation operator**, is defined as:

$$c_i : \mathcal{F}_{N+1} \rightarrow \mathcal{F}_N \quad (1.3.29)$$

$$|n_1, \dots, n_i + 1, \dots\rangle \mapsto (-1)^{s_i} \sqrt{n_i + 1} |n_1, \dots, n_i, \dots\rangle \quad (1.3.30)$$

To understand the significance of the  $(-1)^{s_i}$  term, consider:

$$c_j | \underbrace{n_i = 1, \dots, n_k = 1}_{s_i}, n_j = 1 \rangle = -c_j | n_j = 1, n_{i+1} = 1, \dots, n_k = 1, n_i = 1 \rangle \quad (1.3.31)$$

$$= - | \underbrace{n_{i+1} = 1, \dots, n_k = 1}_{s_i-1}, n_i = 1 \rangle \quad (1.3.32)$$

$$= (-1)(-1)^{s_i-1} | n_i = 1, n_{i+1} = 1, \dots, n_k = 1 \rangle \quad (1.3.33)$$

$$= (-1)^{s_i} | n_i = 1, n_{i+1} = 1, \dots, n_k = 1 \rangle \quad (1.3.34)$$

and similarly:

$$c_j | \underbrace{n_i = 1, \dots, n_k = 1}_{s_i} \rangle = | n_j = 1, n_i = 1, \dots, n_k = 1 \rangle \quad (1.3.35)$$

$$= (-1)^{s_i} | n_i = 1, \dots, n_k = 1, n_j = 1 \rangle \quad (1.3.36)$$

We see that the definition of the fermionic creation and annihilation operators still have the action of creating and annihilating fermions, but now taking exchange degeneracy into account.

Therefore:

$$|n_i = 1, n_j = 0\rangle = |n_j = 0, n_i = 1\rangle, \text{ and } |n_i = 1, n_j = 1\rangle = -|n_j = 1, n_i = 1\rangle \quad (1.3.37)$$

so that:

$$c_i c_j^\dagger |n_i = 1\rangle = c_i |n_j = 1, n_i = 1\rangle = c_i (-|n_i = 1, n_j = 1\rangle) = -|n_j = 1\rangle \quad (1.3.38)$$

which agrees with our definition of  $c_i$  since  $s_j = 1$  and  $s_i = 0$  gives a sign change. Similarly, we have that:

$$c_i c_j |n_i = 1, n_k = 1, n_j = 1\rangle = c_i (-|n_k = 1, n_i = 1\rangle) = c_i (|n_i = 1, n_k = 1\rangle) = |n_k = 1\rangle \quad (1.3.39)$$

which agrees with our definition of  $c_i$  since  $s_j = 2$  and  $s_i = 0$  give no sign changes. We can use

these results (and similar ones) to evaluate the commutation relations for fermionic operators.

We find that if  $i \neq j$ :

$$c_i c_j^\dagger |n_i = 1, n_j = 1\rangle = c_i c_j^\dagger |n_j = 1\rangle = c_i c_j^\dagger |0\rangle = 0 \quad (1.3.40)$$

$$c_j^\dagger c_i |n_i = 1, n_j = 1\rangle = c_j^\dagger c_i |n_j = 1\rangle = c_j^\dagger c_i |0\rangle = 0 \quad (1.3.41)$$

and:

$$c_i c_j^\dagger |n_i = 1\rangle = c_i |n_j = 1, n_i = 1\rangle = -|n_i = 0, n_j = 1\rangle \quad (1.3.42)$$

$$c_j^\dagger c_i |n_i = 1\rangle = c_j^\dagger |0\rangle = |n_j = 1\rangle \quad (1.3.43)$$

while if  $i = j$ :

$$c_i c_i^\dagger |n_i = 1\rangle = 0, \quad c_i c_i^\dagger |0\rangle = |0\rangle \quad (1.3.44)$$

$$c_i^\dagger c_i |n_i = 1\rangle = |n_i = 1\rangle, \quad c_i^\dagger c_i |0\rangle = 0 \quad (1.3.45)$$

$$\iff \{c_i, c_i^\dagger\} = 1 \quad (1.3.46)$$

implying that:

$$\{c_i, c_j^\dagger\} = \delta_{ij} \quad (1.3.47)$$

Similarly, one finds that the only non-zero effect of  $c_i^\dagger c_j^\dagger$  is on the vacuum:

$$c_i^\dagger c_j^\dagger |0\rangle = |n_i = 1, n_j = 1\rangle \quad (1.3.48)$$

$$c_j^\dagger c_i^\dagger |0\rangle = |n_j = 1, n_i = 1\rangle = -|n_i = 1, n_j = 1\rangle \quad (1.3.49)$$

$$\iff \{c_i^\dagger, c_j^\dagger\} = 0, \quad i \neq j \quad (1.3.50)$$

and since  $\{c_i^\dagger, c_i^\dagger\} = 0$ , we find that:

$$\{c_i^\dagger, c_j^\dagger\} = 0 \quad (1.3.51)$$

Therefore:

$$\{c_i^\dagger, c_j^\dagger\}^\dagger = \{c_j, c_i\} = 0 \quad (1.3.52)$$

giving:

$$\{c_i, c_j\} = 0 \quad (1.3.53)$$

These are the anti-commutation relations for fermionic creation/annihilation operators, and are equivalent to the bosonic relations if we replace the anti-commutator by a commutator. Moreover, we may again use these operators to generate the Fock space from the vacuum state  $|0\rangle$ , since:

$$|n_1, n_2, \dots, n_i, \dots\rangle = \frac{1}{\sqrt{n_1! n_2! \dots n_i! \dots}} \prod_{i=1}^N (c_i^\dagger)^{n_i} |0\rangle \quad (1.3.54)$$

where the ordering of the products is as follows:

$$\prod_{i=1}^N (c_i^\dagger)^{n_i} = (c_1^\dagger)^{n_1} (c_2^\dagger)^{n_2} \dots \quad (1.3.55)$$

Finally, the occupation number operator  $\hat{n}_i$  is defined as usual, only that now its eigenvalue spectrum is restricted to 0 and 1, due to the Pauli exclusion principle.

### General summary

In summary, if we define the following generalized commutator:

$$[\hat{A}, \hat{B}]_\eta = \hat{A}\hat{B} - \eta\hat{B}\hat{A} \quad (1.3.56)$$

then the generalized creation/annihilation operators  $a_i^\dagger, a_i$  satisfy the following algebra:

$$[a_i, a_j^\dagger]_\eta = \delta_{ij}, \quad [a_i, a_j]_\eta = [a_i^\dagger, a_j^\dagger]_\eta = 0 \quad (1.3.57)$$

## 1.4 Field operators

The creation and annihilation operators may be used to convert operators in first quantization into **field operators** in second quantization.

In vague terms, a field operator is a field which assigns an operator to every point in real space. If we let  $\{|\psi_i\rangle\}$  be a basis of a Hilbert space equipped with the continuous position basis  $\{|\mathbf{r}\rangle\}$ , then we define:

$$\Psi^\dagger(\mathbf{r}) = \sum_i \psi_i^*(\mathbf{r}) a_i^\dagger, \quad \Psi(\mathbf{r}) = \sum_i \psi_i(\mathbf{r}) a_i \quad (1.4.1)$$

As *Bruus and Flensberg* [4] puts it, these field operators are the linear combination of “all possible ways to add a particle to the system at  $\mathbf{r}$ ”. An important special case of (1.4.1) is when we use the momentum basis  $|\mathbf{k}\rangle = |\psi_i\rangle$  normalized over some volume  $\mathcal{V}$ . Then we find that:

$$\Psi^\dagger(\mathbf{r}) = \frac{1}{\sqrt{\mathcal{V}}} \sum_{\mathbf{k}} e^{-i\mathbf{k}\cdot\mathbf{r}} a_{\mathbf{k}}^\dagger, \quad \Psi(\mathbf{r}) = \frac{1}{\sqrt{\mathcal{V}}} \sum_{\mathbf{k}} e^{i\mathbf{k}\cdot\mathbf{r}} a_{\mathbf{k}} \quad (1.4.2)$$

$$\iff a_{\mathbf{k}}^\dagger = \int e^{i\mathbf{k}\cdot\mathbf{r}} \Psi^\dagger(\mathbf{r}) d\mathbf{r}, \quad a_{\mathbf{k}} = \int e^{-i\mathbf{k}\cdot\mathbf{r}} \Psi(\mathbf{r}) d\mathbf{r} \quad (1.4.3)$$

where we used the fact that:

$$\int e^{-i(\mathbf{k}-\mathbf{q})\cdot\mathbf{r}} d\mathbf{r} = \mathcal{V} \delta_{\mathbf{k}\mathbf{q}} \quad (1.4.4)$$

Clearly, these represent Fourier transform relations between the creation/annihilation operators and the field operators.

It is easy to see that:

$$[\Psi(\mathbf{r}_1), \Psi^\dagger(\mathbf{r}_2)]_\eta = \frac{1}{V} \left[ \sum_{\mathbf{k}} e^{i\mathbf{k}\cdot\mathbf{r}_1} a_{\mathbf{k}}, \sum_{\mathbf{q}} e^{-i\mathbf{q}\cdot\mathbf{r}_2} a_{\mathbf{q}}^\dagger \right]_\eta \quad (1.4.5)$$

$$= \frac{1}{V} \sum_{\mathbf{kq}} e^{i(\mathbf{k}\cdot\mathbf{r}_1 - \mathbf{q}\cdot\mathbf{r}_2)} [a_{\mathbf{k}}, a_{\mathbf{q}}^\dagger]_\eta \quad (1.4.6)$$

$$= \sum_{\mathbf{k}} e^{i\mathbf{k}\cdot(\mathbf{r}_2 - \mathbf{r}_1)} \quad (1.4.7)$$

$$= \delta(\mathbf{r}_2 - \mathbf{r}_1) \quad (1.4.8)$$

and similarly

$$[\Psi(\mathbf{r}_1), \Psi(\mathbf{r}_2)]_\eta = [\Psi^\dagger(\mathbf{r}_1), \Psi^\dagger(\mathbf{r}_2)]_\eta = 0 \quad (1.4.9)$$

### Representing single-body operators

Consider a single particle operator  $\hat{f}$  acting on  $\mathcal{H}$ . In the full product space  $\mathcal{H}^N$ , then we would define:

$$\hat{f} = \mathbb{1} \otimes \mathbb{1} \otimes \dots \otimes \hat{f} \otimes \mathbb{1} \dots \quad (1.4.10)$$

to be the single particle operator acting on the  $i$ th particle Hilbert space. Taking the sum over all particles, we recover the one-body operator:

$$\hat{F} = \sum_i \hat{f}_i \quad (1.4.11)$$

which in a  $\{|i\rangle\}$  basis of  $\mathcal{H}$  reads:

$$\hat{F} = \sum_{k,l} f_{kl} \sum_q |k\rangle_q \langle l|_q, \quad f_{kl} = \langle k|\hat{f}|l\rangle \quad (1.4.12)$$

Our goal is to second quantize the expression  $\sum_q |k\rangle_q \langle l|_q$ , and do so by investigating its effect on some fock state  $|n_i, n_j, \dots\rangle$ . We find that in first quantization:

$$\sum_q |k\rangle_q \langle l|_q \sqrt{\frac{N!}{n_i! n_j! \dots}} \hat{S}_\pm \left( \bigotimes_{m=1}^{n_i} |i\rangle_m \right) \otimes \left( \bigotimes_{m=1}^{n_j} |j\rangle_{n_i+m} \right) \dots \quad (1.4.13)$$

$$= \sqrt{\frac{N!}{n_i! n_j! \dots}} \hat{S}_\pm \sum_q |k\rangle_q \langle l|_q \left( \bigotimes_{m=1}^{n_j} |i\rangle_m \right) \otimes \left( \bigotimes_{m=1}^{n_2} |j\rangle_{n_i+m} \right) \dots \quad (1.4.14)$$

since  $\hat{F}$  is exchange invariant, and therefore commutes with  $\hat{S}_\pm$ .

We can expand the sum in  $q$  to find that (we omit  $\otimes$  to save space):

$$q = 1 : |k\rangle_1 \langle l|i\rangle_1 |i\rangle_2 \dots |i\rangle_{n_i} |j\rangle_{n_i+1} \dots |j\rangle_{n_i+n_j} \dots |u\rangle_q \dots \quad (1.4.15)$$

$$q = 2 : + |i\rangle_1 |k\rangle_2 \langle l|i\rangle_2 |i_3\rangle \dots |i\rangle_{n_i} |j\rangle_{n_i+1} \dots |j\rangle_{n_i+n_j} \dots |u\rangle_q \dots \quad (1.4.16)$$

$$+ \dots \quad (1.4.17)$$

$$q : + |i\rangle_1 |i\rangle_2 \dots |i\rangle_{n_i} |j\rangle_{n_i+1} \dots |k\rangle_q \langle l|u\rangle_q \dots \quad (1.4.18)$$

$$+ \dots \quad (1.4.19)$$

In the  $q$ th line, we will get that  $|u\rangle_q \rightarrow \delta_{lu} |k\rangle_q$ , where  $|u\rangle_q$  is whatever state is in the  $q$ th position. Consequently, the only lines that will survive will be the ones with state  $|l\rangle_q$  in the appropriate position  $q$ . Since there will be  $n_l$  particles in the state  $|l\rangle$ , this will lead to  $n_l$  lines not vanishing. Each of these lines will also be some permutation of  $|i\rangle_1 |i\rangle_2 \dots |i\rangle_{n_i} |j\rangle_{n_i+1} \dots |k\rangle_q \dots$ , and since  $\hat{S}_\pm$  commutes with  $\hat{P}_\sigma$  for any  $\sigma \in S_N$ , we find that:

$$\sum_q |k\rangle_q \langle l|_q \sqrt{\frac{N!}{n_i! n_j! \dots}} \hat{S}_\pm \left( \bigotimes_{m=1}^{n_i} |i\rangle_m \right) \otimes \left( \bigotimes_{m=1}^{n_j} |j\rangle_{n_i+m} \right) \dots \quad (1.4.20)$$

$$= n_l \sqrt{\frac{N!}{n_i! n_j! \dots}} \hat{S}_\pm |i\rangle_1 |i\rangle_2 \dots |i\rangle_{n_i} |j\rangle_{n_i+1} \dots |k\rangle_q \dots \quad (1.4.21)$$

and since:

$$|n_i, \dots, n_l - 1, \dots, n_k + 1, \dots\rangle = \sqrt{\frac{N!}{n_i! \dots (n_l - 1)! \dots (n_k + 1)! \dots}} \hat{S}_\pm |i\rangle_1 |i\rangle_2 \dots |i\rangle_{n_i} |j\rangle_{n_i+1} \dots |k\rangle_q \dots \quad (1.4.22)$$

we find that:

$$\sum_q |k\rangle_q \langle l|_q |n_i, \dots, n_l, \dots, n_k, \dots\rangle \quad (1.4.23)$$

$$= n_l \sqrt{\frac{N!}{n_i! n_j! \dots}} \hat{S}_\pm |i\rangle_1 |i\rangle_2 \dots |i\rangle_{n_i} |j\rangle_{n_i+1} \dots |k\rangle_q \dots \quad (1.4.24)$$

$$= n_l \sqrt{\frac{N!}{n_i! \dots n_l! \dots n_k! \dots}} \sqrt{\frac{n_i! \dots (n_l - 1)! \dots (n_k + 1)! \dots}{N!}} |n_i, \dots, n_l - 1, \dots, n_k + 1, \dots\rangle \quad (1.4.25)$$

$$= \sqrt{n_l} \sqrt{n_k + 1} |n_i, \dots, n_l - 1, \dots, n_k + 1, \dots\rangle \quad (1.4.26)$$

$$= a_k^\dagger a_l |n_i, \dots, n_l, \dots, n_k, \dots\rangle \quad (1.4.27)$$

Finally, we get the very elegant representation of a one-body operator:

$$\hat{F} = \sum_{kl} f_{kl} \hat{a}_k^\dagger \hat{a}_l \quad (1.4.28)$$

If we are working in a Hilbert space embedded with a position representation then we may also

write that:

$$\hat{F} = \sum_{kl} f_{kl} \hat{a}_k^\dagger \hat{a}_l = \sum_{kl} \int \psi_k^*(\mathbf{r}) \hat{f} \psi_l(\mathbf{r}) d\mathbf{r} \hat{a}_k^\dagger \hat{a}_l = \int \Psi_k^*(\mathbf{r}) \hat{f} \Psi_l(\mathbf{r}) d\mathbf{r} \quad (1.4.29)$$

### Representing two-body operators

We begin by deriving a useful property of creation/annihilation operators. Firstly note that the commutator algebra for these operators may be written as:

$$a_k a_j^\dagger = \eta a_j^\dagger a_k + \delta_{jk}, \quad a_k a_l = \eta a_l a_k \quad (1.4.30)$$

where  $\eta = 1$  for bosons and  $\eta = -1$  for fermions. Then:

$$a_i^\dagger a_k a_j^\dagger a_l = a_i^\dagger (\eta a_j^\dagger a_k + \delta_{jk}) a_l \quad (1.4.31)$$

$$= \eta a_i^\dagger a_j^\dagger a_k a_l + \delta_{jk} a_i^\dagger a_l \quad (1.4.32)$$

$$= \eta^2 a_i^\dagger a_j^\dagger a_l a_k + \delta_{jk} a_i^\dagger a_l \quad (1.4.33)$$

$$= a_i^\dagger a_j^\dagger a_l a_k + \delta_{jk} a_i^\dagger a_l \quad (1.4.34)$$

Now consider a two-body operator written as  $\hat{g}_{qq'} = \hat{f}_q \hat{h}'_q$  where  $\hat{f}_q$  acts on  $\mathcal{H}_q$  and  $\hat{g}_{q'}$  acts on  $\mathcal{H}_{q'}$ . Then, we find that the total two-body operator may be written as:

$$\hat{G} = \frac{1}{2} \sum_{q \neq q'} \hat{g}_{qq'} \quad (1.4.35)$$

where  $\frac{1}{2}$  takes care of double counting, and we discard  $q = q'$  terms since a two-body operator must involve two different particles.

Therefore:

$$\hat{G} = \frac{1}{2} \sum_{q \neq q'} \hat{g}_{qq'} = \frac{1}{2} \left( \sum_q \hat{f}_q \sum_{q'} \hat{g}_{q'} - \sum_q \hat{f}_q \hat{g}_q \right) \quad (1.4.36)$$

$$= \frac{1}{2} \left( \hat{F} \hat{G} - \sum_q \hat{f}_q \hat{g}_q \right) \quad (1.4.37)$$

$$(1.4.38)$$

Now we use the fact that  $\hat{F} = \sum_q \hat{f}_q$ ,  $\hat{G} = \sum_{q'} \hat{f}_{q'}$  and  $\sum_q \hat{f}_q \hat{g}_q$  are single-body operators, and thus

have a field representation of the type in (1.4.28):

$$\hat{G} = \frac{1}{2} \left( \sum_{ik} f_{ik} a_i^\dagger a_k \sum_{jl} g_{jl} a_j^\dagger a_l - \sum_{il} (fh)_{il} a_i^\dagger a_l \right) \quad (1.4.39)$$

$$= \frac{1}{2} \left( \sum_{ijkl} f_{ik} g_{jl} a_i^\dagger a_k a_j^\dagger a_l - \sum_{il} (fh)_{il} a_i^\dagger a_l \right) \quad (1.4.40)$$

$$= \frac{1}{2} \left( \sum_{ijkl} f_{ik} g_{jl} a_i^\dagger a_j^\dagger a_l a_k + \sum_{ikjl} f_{ik} g_{jl} \delta_{jk} a_i^\dagger a_l - \sum_{il} (fh)_{il} a_i^\dagger a_l \right) \quad (1.4.41)$$

$$= \frac{1}{2} \left( \sum_{ijkl} f_{ik} g_{jl} a_i^\dagger a_j^\dagger a_l a_k + \sum_{ijl} f_{ij} g_{jl} a_i^\dagger a_l - \sum_{ijl} f_{ij} h_{jl} a_i^\dagger a_l \right) \quad (1.4.42)$$

$$= \frac{1}{2} \sum_{ijkl} f_{ik} g_{jl} a_i^\dagger a_j^\dagger a_l a_k \quad (1.4.43)$$

Note that the matrix elements of  $\hat{g}, \hat{f}, \hat{h}$  are related by:

$$g_{ijkl} = \langle i|_q \langle j|_{q'} |\hat{g}| |k\rangle_q |l\rangle_{q'} = \langle i|_{q'} \langle j|_q |\hat{f}_q \hat{h}'_q| |k\rangle_q |l\rangle_{q'} = f_{ik} g_{jl} \quad (1.4.44)$$

so that:

$$\hat{G} = \frac{1}{2} \sum_{ijkl} g_{ijkl} a_i^\dagger a_j^\dagger a_l a_k \quad (1.4.45)$$

Luckily, any two-body operator may be expanded as a power series in one-particle operators:

$$G = \sum_{\alpha\beta} c_{\alpha\beta} \sum_{q \neq q'} \hat{f}_q^\alpha \hat{h}_{q'}^\beta \quad (1.4.46)$$

$$= \frac{1}{2} \sum_{ikjl} (f^\alpha)_{ik} (g^\beta)_{jl} a_i^\dagger a_j^\dagger a_l a_k \quad (1.4.47)$$

$$= \frac{1}{2} \sum_{ikjl} g_{ijkl} a_i^\dagger a_j^\dagger a_l a_k \quad (1.4.48)$$

## Change of basis

Finally, we must comment on how changes of basis affect the field representations we have derived. We have already observed that the change from the position to the momentum basis is given by a Fourier transform.

More generally, we have that given two bases  $\{|u_i\rangle\}$  and  $\{|v_i\rangle\}$  of  $\mathcal{H}$ . Then, for any  $|\psi\rangle \in \mathcal{H}$ :

$$\hat{a}_{u_i}^\dagger |0\rangle = |u_i\rangle = \sum_j \langle v_j | u_i \rangle |v_j\rangle = \sum_j \langle v_j | u_i \rangle \hat{a}_{v_j}^\dagger |0\rangle \quad (1.4.49)$$

implying that:

$$a_{u_i}^\dagger = \sum_j \langle v_j | u_i \rangle a_{v_j}^\dagger \implies a_{u_i} = \sum_j \langle u_i | v_j \rangle a_{v_j} \quad (1.4.50)$$

Clearly, we see that using  $\{|u_i\rangle\} = \{|\mathbf{r}\rangle\}$  then  $\hat{a}_{\mathbf{r}} = \sum_j \langle \mathbf{r} | v_j \rangle a_{v_j}$  which is just the field operator  $\Psi(\mathbf{r})$  we defined earlier.

Using a change of basis allows us to derive in a much simpler way the field representation of diagonalizable operators. Indeed, suppose we have some one-body operator  $\hat{f}$  with eigenbasis  $\{|\psi_i\rangle\}$  and eigenvectors  $\lambda_i$ . Then:

$$\hat{F} = \sum_i \lambda_i \hat{n}_i = \sum_i \lambda_i a_{\psi_i}^\dagger a_{\psi_i} \quad (1.4.51)$$

Consequently, using another basis  $\{|\phi_j\rangle\}$  then

$$\hat{F} = \sum_i \lambda_i a_{\psi_i}^\dagger a_{\psi_i} = \sum_i \lambda_i \sum_k \langle \phi_k | \psi_i \rangle a_{\phi_k}^\dagger \sum_j \langle \psi_i | \phi_j \rangle a_{\phi_j} \quad (1.4.52)$$

$$= \sum_{ikj} \langle \phi_k | \psi_i \rangle \langle \psi_i | \hat{f} | \psi_i \rangle \langle \psi_i | \phi_j \rangle a_{\phi_k}^\dagger a_{\phi_j} \quad (1.4.53)$$

$$= \sum_{kj} \langle \phi_k | \hat{f} | \phi_j \rangle a_{\phi_k}^\dagger a_{\phi_j} \quad (1.4.54)$$

$$= \sum_{kj} f_{kj} a_{\phi_k}^\dagger a_{\phi_j} \quad (1.4.55)$$

as we found earlier. Similar arguments may be used to show that for two-body operators  $\hat{G}$ :

$$\hat{G} = \frac{1}{2} \sum_{ikjl} g_{ijkl} a_i^\dagger a_j^\dagger a_l a_k \quad (1.4.56)$$

## 1.5 Quantising the electromagnetic field

For non-relativistic systems we typically use the Coulomb gauge  $\nabla \cdot \mathbf{A} = 0$ , so that in vacuum the electric and magnetic fields are given by:

$$\mathbf{B} = \nabla \times \mathbf{A} \quad (1.5.1)$$

$$\mathbf{E} = -\frac{\partial \mathbf{A}}{\partial t} \quad (1.5.2)$$

Inserting these into the Ampere-Maxwell law we find that:

$$\nabla^2 \mathbf{A} = \frac{1}{c^2} \frac{\partial^2 \mathbf{A}}{\partial t^2} \quad (1.5.3)$$

which is the classical wave-equation. If we take  $\mathbf{A}$  to be in a box of volume  $\mathcal{V}$  with periodic boundary conditions, then the solutions to the above will be those of a waveguide, and can thus be expanded into modes:

$$\mathbf{A}(\mathbf{r}, t) = \sum_{\mathbf{k}} \mathbf{A}_{\mathbf{k}}(t) e^{i\mathbf{k} \cdot \mathbf{r}} \quad (1.5.4)$$

which when substituted into (1.5.3) yields:

$$\mathbf{A}(\mathbf{r}, t) = \sum_{\mathbf{k}} (\mathbf{A}_{\mathbf{k}}^+ e^{i\omega_{\mathbf{k}} t} + \mathbf{A}_{\mathbf{k}}^- e^{-i\omega_{\mathbf{k}} t}) e^{i\mathbf{k} \cdot \mathbf{r}} \quad (1.5.5)$$

$$= \sum_{\mathbf{k}} (\mathbf{A}_{-\mathbf{k}}^+ e^{-i(\mathbf{k} \cdot \mathbf{r} - \omega_{\mathbf{k}} t)} + \mathbf{A}_{\mathbf{k}}^- e^{i(\mathbf{k} \cdot \mathbf{r} - \omega_{\mathbf{k}} t)}) \quad (1.5.6)$$

Since the vector potential must be a real quantity, we must have that:

$$\sum_{\mathbf{k}} (\mathbf{A}_{-\mathbf{k}}^+ e^{-i(\mathbf{k} \cdot \mathbf{r} - \omega_{\mathbf{k}} t)} + \mathbf{A}_{\mathbf{k}}^- e^{i(\mathbf{k} \cdot \mathbf{r} - \omega_{\mathbf{k}} t)}) = \sum_{\mathbf{k}} ((\mathbf{A}_{-\mathbf{k}}^+)^* e^{i(\mathbf{k} \cdot \mathbf{r} - \omega_{\mathbf{k}} t)} + (\mathbf{A}_{\mathbf{k}}^-)^* e^{-i(\mathbf{k} \cdot \mathbf{r} - \omega_{\mathbf{k}} t)}) \quad (1.5.7)$$

so that  $\mathbf{A}_{-\mathbf{k}}^+ = (\mathbf{A}_{\mathbf{k}}^-)^*$ . It follows that we may decompose the vector potential into modes of wave-vector  $\mathbf{k}$  and polarisation  $\epsilon_\lambda$  by letting  $\mathbf{A}_{\mathbf{k}}^- = A_{\mathbf{k},\lambda} \epsilon_\lambda$ :

$$\mathbf{A}(\mathbf{r}, t) = \frac{1}{\sqrt{\mathcal{V}}} \sum_{\mathbf{k}} \sum_{\lambda=1,2} (A_{\mathbf{k},\lambda} e^{i(\mathbf{k} \cdot \mathbf{r} - \omega_{\mathbf{k}} t)} + A_{\mathbf{k},\lambda}^* e^{-i(\mathbf{k} \cdot \mathbf{r} - \omega_{\mathbf{k}} t)}) \epsilon_{\mathbf{k},\lambda} \quad (1.5.8)$$

where  $\{\epsilon_1, \epsilon_2, \mathbf{k}/|\mathbf{k}|\}$  form an orthonormal basis and  $\omega_{\mathbf{k}} = |\mathbf{k}|c$ . The classical hamiltonian for the electromagnetic field is given by

$$\hat{H} = \frac{1}{2} \int (\varepsilon_0 |\mathbf{E}|^2 + \frac{1}{\mu_0} |\mathbf{B}|^2) d\mathbf{r} = \frac{1}{2} \int \left( \varepsilon_0 \left| \frac{\partial \mathbf{A}}{\partial t} \right|^2 + \frac{1}{\mu_0} |\nabla \times \mathbf{A}|^2 \right) d\mathbf{r} \quad (1.5.9)$$

We now use some Fourier analysis trickery to simplify the above expression. Firstly, note that by applying Parseval's theorem (not to be confused with Parseval's *identity*), which states that:

$$\int |f(\mathbf{r})|^2 d\mathbf{r} = \frac{1}{\sqrt{\mathcal{V}}} \sum_{\mathbf{k}} |\tilde{f}(\mathbf{k})|^2 \quad (1.5.10)$$

then we get (we ignore any prefactors in front of the sum as we will normalize everything at the end):

$$\int \left| \frac{\partial \mathbf{A}}{\partial t} \right|^2 d\mathbf{r} = \sum_{\mathbf{k}} \left| \mathcal{F} \left( \frac{\partial \mathbf{A}}{\partial t} \right) \right|^2, \quad \int |\nabla \times \mathbf{A}|^2 d\mathbf{r} = \sum_{\mathbf{k}} \left| \mathcal{F}(\nabla \times \mathbf{A}) \right|^2 \quad (1.5.11)$$

Computing the Fourier transform is immediate:

$$\mathcal{F}(\nabla \times \mathbf{A})(\mathbf{k}') = \sum_{\mathbf{k}, \lambda} (i\mathbf{k} \times \epsilon_{\mathbf{k}, \lambda}) (A_{\mathbf{k}, \lambda} e^{-i\omega_{\mathbf{k}} t} \delta_{\mathbf{k}'} - A_{\mathbf{k}, \lambda}^* e^{i\omega_{\mathbf{k}} t} \delta_{-\mathbf{k}'}) \quad (1.5.12)$$

$$\mathcal{F} \left( \frac{\partial \mathbf{A}}{\partial t} \right)(\mathbf{k}') = \sum_{\mathbf{k}, \lambda} (i\omega_{\mathbf{k}}) (A_{\mathbf{k}, \lambda} e^{-i\omega_{\mathbf{k}} t} \delta_{\mathbf{k}'} - A_{\mathbf{k}, \lambda}^* e^{i\omega_{\mathbf{k}} t} \delta_{-\mathbf{k}'}) \epsilon_{\mathbf{k}, \lambda} \quad (1.5.13)$$

where  $\delta_{\mathbf{k}'}$  is shorthand for  $\delta_{\mathbf{k}', \mathbf{k}}$ . We also note that:

$$\epsilon_{\mathbf{k}, \lambda} \cdot \epsilon_{t\mathbf{k}, \epsilon'_\lambda} = \delta_{\lambda, \lambda'} \quad (1.5.14)$$

and<sup>2</sup>

$$(i\mathbf{k} \times \epsilon_\lambda) \cdot (-i\mathbf{k} \times \epsilon_{\lambda'}) = |\mathbf{k}|^2 \delta_{\lambda, \lambda'} \quad (1.5.15)$$

---

<sup>2</sup>this is easy to prove:

$$\begin{aligned} (\mathbf{a} \times \mathbf{b}) \cdot (\mathbf{a} \times \mathbf{c}) &= \epsilon_{ijk} a_j b_k \epsilon_{imn} a_m c_n \\ &= (\delta_{jm} \delta_{kn} - \delta_{jn} \delta_{km}) a_j a_m b_k c_n \\ &= |\mathbf{a}|^2 (\mathbf{b} \cdot \mathbf{c}) - (\mathbf{a} \cdot \mathbf{c})(\mathbf{a} \cdot \mathbf{b}) \end{aligned}$$

and since  $\mathbf{b} = \epsilon_\lambda$  is orthonormal to  $\mathbf{c} = \epsilon_{\lambda'}$ , and since  $\mathbf{k}$  is orthogonal to both polarization vectors, we get the desired result.

so that

$$\sum_{\mathbf{k}'} |\mathcal{F}(\nabla \times \mathbf{A})|^2 = \sum_{\mathbf{k}, \mathbf{k}', \lambda, \lambda'} (i\mathbf{k} \times \boldsymbol{\epsilon}_\lambda) \cdot (-i\mathbf{k} \times \boldsymbol{\epsilon}_{\lambda'}) (A_{\mathbf{k}, \lambda} e^{-i\omega_{\mathbf{k}} t} \delta_{\mathbf{k}'} - A_{\mathbf{k}, \lambda}^* e^{i\omega_{\mathbf{k}} t} \delta_{-\mathbf{k}'}) \\ (A_{\mathbf{k}, \lambda'}^* e^{i\omega_{\mathbf{k}} t} \delta_{\mathbf{k}'} - A_{\mathbf{k}, \lambda'} e^{-i\omega_{\mathbf{k}} t} \delta_{-\mathbf{k}'}) \quad (1.5.16)$$

$$= \sum_{\mathbf{k}, \lambda} |\mathbf{k}|^2 (2|A_{\mathbf{k}, \lambda}|^2 - A_{\mathbf{k}, \lambda} A_{\mathbf{k}, \lambda} e^{-2i\omega_{\mathbf{k}} t} - A_{\mathbf{k}, \lambda}^* A_{\mathbf{k}, \lambda}^* e^{2i\omega_{\mathbf{k}} t}) \quad (1.5.17)$$

and similarly:

$$\sum_{\mathbf{k}'} \left| \mathcal{F} \left( \frac{\partial \mathbf{A}}{\partial t} \right) \right|^2 = \sum_{\mathbf{k}, \mathbf{k}', \lambda, \lambda'} (i\omega)(-i\omega) (A_{\mathbf{k}, \lambda} e^{-i\omega_{\mathbf{k}} t} - A_{\mathbf{k}, \lambda}^* e^{i\omega_{\mathbf{k}} t}) (A_{\mathbf{k}, \lambda} e^{-i\omega_{\mathbf{k}} t} - A_{\mathbf{k}, \lambda}^* e^{i\omega_{\mathbf{k}} t}) \boldsymbol{\epsilon}_\lambda \cdot \boldsymbol{\epsilon}_{\lambda'} \\ = \sum_{\mathbf{k}, \lambda} \omega_{\mathbf{k}}^2 (2|A_{\mathbf{k}, \lambda}|^2 + A_{\mathbf{k}, \lambda} A_{\mathbf{k}, \lambda} e^{-2i\omega_{\mathbf{k}} t} + A_{\mathbf{k}, \lambda}^* A_{\mathbf{k}, \lambda}^* e^{2i\omega_{\mathbf{k}} t})$$

Finally, we find that (we switch  $\mathbf{k}' \rightarrow \mathbf{k}$  for convenience):

$$\hat{H} = 2\varepsilon_0 \sum_{\mathbf{k}, \lambda} \omega_{\mathbf{k}}^2 |A_{\mathbf{k}, \lambda}|^2 = 2\varepsilon_0 \sum_{\mathbf{k}, \lambda} \omega_{\mathbf{k}}^2 (|A_{\mathbf{k}, \lambda}^R|^2 + |A_{\mathbf{k}, \lambda}^I|^2) \quad (1.5.18)$$

where  $A_{\mathbf{k}, \lambda} = A_{\mathbf{k}, \lambda}^R + iA_{\mathbf{k}, \lambda}^I$ . Note that if we define  $A_{\mathbf{k}, \lambda}(t) = A_{\mathbf{k}, \lambda} e^{-i\omega_{\mathbf{k}} t}$  then:

$$\dot{A}_{\mathbf{k}, \lambda}^R = \omega_{\mathbf{k}} A_{\mathbf{k}, \lambda}^I, \quad \dot{A}_{\mathbf{k}, \lambda}^I = -\omega_{\mathbf{k}} A_{\mathbf{k}, \lambda}^R \quad (1.5.19)$$

and thus:

$$\frac{\partial H}{\partial A_{\mathbf{k}, \lambda}^R} = 4\varepsilon_0 \omega_{\mathbf{k}}^2 A_{\mathbf{k}, \lambda}^R = -4\varepsilon_0 \omega_{\mathbf{k}} \dot{A}_{\mathbf{k}, \lambda}^I \quad (1.5.20)$$

$$\frac{\partial H}{\partial A_{\mathbf{k}, \lambda}^I} = 4\varepsilon_0 \omega_{\mathbf{k}}^2 A_{\mathbf{k}, \lambda}^I = 4\varepsilon_0 \omega_{\mathbf{k}} \dot{A}_{\mathbf{k}, \lambda}^R \quad (1.5.21)$$

implying that  $A_{\mathbf{k}, \lambda}^R$  and  $A_{\mathbf{k}, \lambda}^I$  are canonically conjugate variables (up to some proportionality constant). So, we may define the conjugate position and conjugate momenta to be:

$$Q_{\mathbf{k}, \lambda} = 2\sqrt{\varepsilon_0} A_{\mathbf{k}, \lambda}^R \quad (1.5.22)$$

$$P_{\mathbf{k}, \lambda} = 2\omega_{\mathbf{k}} \sqrt{\varepsilon_0} A_{\mathbf{k}, \lambda}^I \quad (1.5.23)$$

respectively. Clearly, these satisfy:

$$\begin{cases} \dot{Q}_{\mathbf{k}, \lambda} = P_{\mathbf{k}, \lambda} \\ \dot{P}_{\mathbf{k}, \lambda} = -\omega_{\mathbf{k}}^2 Q_{\mathbf{k}, \lambda} \end{cases} \quad \begin{cases} \frac{\partial H}{\partial Q_{\mathbf{k}, \lambda}} = -\dot{P}_{\mathbf{k}, \lambda} \\ \frac{\partial H}{\partial P_{\mathbf{k}, \lambda}} = \dot{Q}_{\mathbf{k}, \lambda} \end{cases} \quad (1.5.24)$$

as would be the case for a harmonic oscillator. Consequently, also the hamiltonian will be identical to that of a harmonic oscillator:

$$H = \frac{1}{2} \sum_{\mathbf{k}, \lambda} (P_{\mathbf{k}, \lambda}^2 + \omega_{\mathbf{k}}^2 Q_{\mathbf{k}, \lambda}^2) \quad (1.5.25)$$

We can now quantize the electromagnetic field just as one would quantize the harmonic oscillator. We promote  $P_{\mathbf{k},\lambda}$  and  $Q_{\mathbf{k},\lambda}$  to quantum operators  $\hat{p}_{\mathbf{k},\lambda}$  and  $\hat{q}_{\mathbf{k},\lambda}$  which satisfy the canonical commutation relations:

$$[\hat{q}_{\mathbf{k},\lambda}, \hat{p}_{\mathbf{k}',\lambda'}] = i\hbar\delta_{\mathbf{k}\mathbf{k}'}\delta_{\lambda\lambda'} \quad (1.5.26)$$

$$[\hat{q}_{\mathbf{k},\lambda}, \hat{q}_{\mathbf{k}',\lambda'}] = [\hat{p}_{\mathbf{k},\lambda}, \hat{p}_{\mathbf{k}',\lambda'}] = 0 \quad (1.5.27)$$

so that:

$$\hat{H} = \frac{1}{2} \sum_{\mathbf{k},\lambda} (\hat{p}_{\mathbf{k},\lambda}^2 + \omega_{\mathbf{k}}^2 \hat{q}_{\mathbf{k},\lambda}^2) \quad (1.5.28)$$

We introduce the ladder operators:

$$\begin{cases} a_{\mathbf{k},\lambda}^\dagger = \sqrt{\frac{\hbar}{2\omega_{\mathbf{k}}}} (\omega_{\mathbf{k}} \hat{q}_{\mathbf{k},\lambda} - i \hat{p}_{\mathbf{k},\lambda}) \\ a_{\mathbf{k},\lambda} = \sqrt{\frac{\hbar}{2\omega_{\mathbf{k}}}} (\omega_{\mathbf{k}} \hat{q}_{\mathbf{k},\lambda} + i \hat{p}_{\mathbf{k},\lambda}) \end{cases} \implies \begin{cases} \hat{q}_{\mathbf{k},\lambda} = \sqrt{\frac{\hbar}{2\omega_{\mathbf{k}}}} (a_{\mathbf{k},\lambda}^\dagger + a_{\mathbf{k},\lambda}) \\ \hat{p}_{\mathbf{k},\lambda} = i \sqrt{\frac{\hbar\omega_{\mathbf{k}}}{2}} (a_{\mathbf{k},\lambda}^\dagger - a_{\mathbf{k},\lambda}) \end{cases} \quad (1.5.29)$$

With these new operators, the Hamiltonian turns into the familiar quantum harmonic oscillator:

$$\hat{H} = \hbar\omega_{\mathbf{k}} \sum_{\mathbf{k},\lambda} \left( a_{\mathbf{k},\lambda}^\dagger a_{\mathbf{k},\lambda} + \frac{1}{2} \right) \quad (1.5.30)$$

Finally, to relate this hamiltonian to our classical expression (1.5.8) of the vector potential, we make use of the fact that:

$$A_{\mathbf{k},\lambda} = \frac{1}{2\sqrt{\varepsilon_0}} \sqrt{\frac{\hbar}{2\omega_{\mathbf{k}}}} (a_{\mathbf{k},\lambda}^\dagger + a_{\mathbf{k},\lambda}) + \frac{i}{2\sqrt{\varepsilon_0}\omega_{\mathbf{k}}} i \sqrt{\frac{\hbar\omega_{\mathbf{k}}}{2}} (a_{\mathbf{k},\lambda}^\dagger - a_{\mathbf{k},\lambda}) \quad (1.5.31)$$

$$= \sqrt{\frac{\hbar}{2\varepsilon_0\omega_{\mathbf{k}}}} a_{\mathbf{k},\lambda} \implies A_{\mathbf{k},\lambda}^\dagger = \sqrt{\frac{\hbar}{2\varepsilon_0\omega_{\mathbf{k}}}} a_{\mathbf{k},\lambda}^\dagger \quad (1.5.32)$$

giving:

$$\mathbf{A}(\mathbf{r}, t) = \sqrt{\frac{\hbar}{2\varepsilon_0\omega_{\mathbf{k}}\mathcal{V}}} \sum_{\mathbf{k}} \sum_{\lambda=1,2} (e^{i(\mathbf{k}\cdot\mathbf{r}-\omega_{\mathbf{k}}t)} a_{\mathbf{k},\lambda} + e^{-i(\mathbf{k}\cdot\mathbf{r}-\omega_{\mathbf{k}}t)} a_{\mathbf{k},\lambda}^\dagger) \boldsymbol{\epsilon}_\lambda \quad (1.5.33)$$

$$\mathbf{E}(\mathbf{r}, t) = i \sqrt{\frac{\hbar\omega_{\mathbf{k}}}{2\varepsilon_0\mathcal{V}}} \sum_{\mathbf{k}} \sum_{\lambda=1,2} (e^{i(\mathbf{k}\cdot\mathbf{r}-\omega_{\mathbf{k}}t)} a_{\mathbf{k},\lambda} - e^{-i(\mathbf{k}\cdot\mathbf{r}-\omega_{\mathbf{k}}t)} a_{\mathbf{k},\lambda}^\dagger) \boldsymbol{\epsilon}_\lambda \quad (1.5.34)$$

$$\mathbf{B}(\mathbf{r}, t) = i \sqrt{\frac{\hbar}{2\varepsilon_0\omega_{\mathbf{k}}\mathcal{V}}} \sum_{\mathbf{k}} \sum_{\lambda=1,2} (e^{i(\mathbf{k}\cdot\mathbf{r}-\omega_{\mathbf{k}}t)} a_{\mathbf{k},\lambda} - e^{-i(\mathbf{k}\cdot\mathbf{r}-\omega_{\mathbf{k}}t)} a_{\mathbf{k},\lambda}^\dagger) (\mathbf{k} \times \boldsymbol{\epsilon}_\lambda) \quad (1.5.35)$$

# CHAPTER 2

---

## Deriving the Hubbard models

### 2.1 Introduction

The Hubbard hamiltonians are a class of strongly correlated models which capture the essential physics required to investigate interacting bosons and fermions in solids. We can distinguish between the various Hubbard models as follows:

1. Bose-Hubbard model
2. Fermi-Hubbard model
3. Extended-Bose Hubbard model
4. Extended-Fermi Hubbard model

The original Fermi-Hubbard model was first introduced by John Hubbard in a seminal series of papers [16–21] in the 1960s to investigate the behaviour of electrons in narrow bands. Hubbard considered a generalization of the tight-binding approximation, which allows electrons to hop between nearest neighbor orbitals, by including a contact potential  $U$ , known as a Hubbard potential, which acts on fermions residing on the same orbital. Since then, the Fermi Hubbard model has been modified into the Bose Hubbard model to describe spinless bosons [12], and has been extended into the Extended Hubbard models to include longer range interactions.

Despite their simplicity the Hubbard models are very hard to solve exactly. Analytical methods such as the Bethe ansatz are only successful in one dimension, and even then only for the Fermi-Hubbard model which was solved by Lieb and Wu in 1968 [28]. Nevertheless, the model has been immensely powerful in describing phenomena which traditional band theory was ill-equipped for. One such famous example is the existence of Mott insulators [6, 29], materials that satisfy the typical requirements to be conductive (namely partially filled bands), but which still exhibit insulating behaviour.

Interest in the Hubbard model has been further fuelled by recent advancements in quantum optics and cold atom experiments. The ability to load quantum gases on optical lattices has allowed physicists to probe condensed matter models with unprecedented tunability [3]. Superfluid to Mott

insulator transitions in boson gases were first observed in a landmark paper [13] by *Greiner et al.* in 2002, four years after such an experiment was first proposed by *Jaksch et al.* [22]. Just a few years later analogous results for fermion gases would be obtained by *Jöerdens et al.* [25].

We begin by presenting a comprehensive derivation of the Hubbard models [10, 22, 23], making use of second quantization.

## 2.2 Derivation for Fermions

We will model a solid as consisting of ions and electrons arranged in a crystal lattice. Due to the significantly larger mass of the ions, and since we will only be focusing on the behaviour of the electrons, we are justified in adopting the Born-Oppenheimer approximation and thus model the ions as forming a fixed, periodic lattice.

The principal dynamics in the Born-Oppenheimer approximation are given by the following hamiltonian:

$$H = H_0 + H_{int} = \sum_i h_i + \sum_{i < j} V_{ee}(\mathbf{r}_j - \mathbf{r}_i) \quad (2.2.1)$$

The single particle hamiltonian is:

$$h_i = \frac{\mathbf{p}_i^2}{2m} + \overbrace{V_I(\mathbf{r}_i)}^{\text{ion potential}} \quad (2.2.2)$$

where  $V_I(\mathbf{r}_i)$  is the periodic potential produced by the ion lattice. Thus it satisfies:

$$V_I(\mathbf{r} + \mathbf{R}) = V_I(\mathbf{r}) \quad (2.2.3)$$

where  $\mathbf{R}$  is a lattice vector. In the tight binding approximation  $H_0$  would be the only relevant term, but as we have seen one must take into account electron-electron interactions in order to explain phenomena such as Mott-insulating phases. Hence, we must also add another interaction term i.e.

$$V_{ee}(\mathbf{r}_j - \mathbf{r}_i) = \frac{e^2}{|\mathbf{r}_j - \mathbf{r}_i|^2} \quad (2.2.4)$$

As we have seen in the previous chapter, there are many difficulties inherent to many body hamiltonians in first quantization. One would therefore wish to derive a second-quantized form of (2.2.1).

We begin by noting that due to the periodicity of  $V$ , the eigenstates  $\phi_{\alpha\mathbf{k}}$  of the single-particle hamiltonian  $h$ :

$$\hat{h}\phi_{n\mathbf{k}}(\mathbf{r}) = \varepsilon_{\alpha\mathbf{k}}\phi_{n\mathbf{k}}(\mathbf{r}) \quad (2.2.5)$$

must be *Bloch states* and thus have the form:

$$\phi_{\alpha\mathbf{k}}(\mathbf{r}) = e^{i\mathbf{k}\mathbf{r}}u_{\alpha\mathbf{k}}(\mathbf{r}), \quad u_{\alpha\mathbf{k}}(\mathbf{r} + \mathbf{R}) = u_{\alpha\mathbf{k}}(\mathbf{r}) \quad (2.2.6)$$

We have denoted the band index by  $\alpha$  and the quasi-momentum in the First Brillouin Zone (FBZ) by  $\mathbf{k}$ .

We can sum over all Bloch states centered at site  $i$  and use Bloch's theorem to create a *Wannier*

state<sup>1</sup>:

$$\psi_\alpha(\mathbf{r} - \mathbf{R}_i) = \frac{1}{\sqrt{L}} \sum_{\mathbf{k}} \phi_{\alpha\mathbf{k}}(\mathbf{r} - \mathbf{R}_i) = \frac{1}{\sqrt{L}} \sum_{\mathbf{k}} e^{-i\mathbf{k}\cdot\mathbf{R}_i} \phi_{\alpha\mathbf{k}}(\mathbf{r}) \quad (2.2.7)$$

$$\iff \phi_{\alpha\mathbf{k}}(\mathbf{r}) = \frac{1}{\sqrt{L}} \sum_i e^{i\mathbf{k}\cdot\mathbf{R}_i} \psi_\alpha(\mathbf{r} - \mathbf{R}_i) \quad (2.2.8)$$

Here  $\mathbf{R}_i$  is the lattice vector pointing to site  $i$ . The analogy between these two bases is self-evident, while Bloch states are localized states in *momentum space*, Wannier states are localized states in *real space*.

Note that Wannier states, like Bloch states, are orthonormal:

$$\int \psi_\alpha^*(\mathbf{r} - \mathbf{R}_i) \psi_\alpha(\mathbf{r} - \mathbf{R}_j) d^3\mathbf{r} = \frac{1}{L} \int \sum_{\mathbf{k}\mathbf{k}'} e^{i\mathbf{k}\cdot\mathbf{R}_i} e^{-i\mathbf{k}\cdot\mathbf{R}_j} \phi_{\alpha\mathbf{k}}(\mathbf{r})^* \phi_{\alpha\mathbf{k}'}(\mathbf{r}) d^3\mathbf{r} \quad (2.2.9)$$

$$= \frac{1}{L} \sum_{\mathbf{k}\mathbf{k}'} e^{i\mathbf{k}\cdot\mathbf{R}_i} e^{-i\mathbf{k}\cdot\mathbf{R}_j} \delta_{\mathbf{k},\mathbf{k}'} \quad (2.2.10)$$

$$= \frac{1}{L} \sum_{\mathbf{k}} e^{-i\mathbf{k}\cdot(\mathbf{R}_j - \mathbf{R}_i)} \quad (2.2.11)$$

$$= \delta_{ij} \quad (2.2.12)$$

Consequently, let us define the creation/annihilation operators  $c_{\alpha i \sigma}^\dagger / c_{\alpha i \sigma}$  that create/annihilate an electron in a Wannier state with spin  $\sigma$  and band index  $n$ . Clearly, we can relate them to  $c_{\alpha\mathbf{k}\sigma}^\dagger / c_{\alpha\mathbf{k}\sigma}$  via:

$$c_{\alpha i \sigma}^\dagger = \frac{1}{\sqrt{L}} \sum_{\mathbf{k}} e^{-i\mathbf{k}\cdot\mathbf{R}_i} c_{\alpha\mathbf{k}\sigma}^\dagger \quad (2.2.13)$$

This allows us to define the field operators:

$$\Psi_\sigma^\dagger(\mathbf{r}) = \sum_{\alpha i} \psi_{\alpha i}^*(\mathbf{r}) c_{\alpha i \sigma}^\dagger = \sum_{\alpha \mathbf{k}} \phi_{\alpha\mathbf{k}}^*(\mathbf{r}) c_{\alpha\mathbf{k}\sigma}^\dagger \quad (2.2.14)$$

$$\Psi_\sigma(\mathbf{r}) = \sum_{\alpha i} \psi_{\alpha i}(\mathbf{r}) c_{\alpha i \sigma}^\dagger = \sum_{\alpha \mathbf{k}} \phi_{\alpha\mathbf{k}}(\mathbf{r}) c_{\alpha\mathbf{k}\sigma}^\dagger \quad (2.2.15)$$

which create/annihilate an electron with spin  $\sigma$  at position  $\mathbf{r}$ .

This finally allows us to second quantize (2.2.1) by writing:

$$H = \sum_{\sigma} \int \Psi_\sigma^\dagger(\mathbf{r}) \left[ \frac{\mathbf{p}^2}{2m} + V_I(\mathbf{r}) \right] \Psi_\sigma(\mathbf{r}) d^3\mathbf{r} \quad (2.2.16)$$

$$+ \frac{1}{2} \sum_{\sigma\sigma'} \iint \Psi_\sigma^\dagger(\mathbf{r}) \Psi_{\sigma'}^\dagger(\mathbf{r}') V_{ee}(\mathbf{r} - \mathbf{r}') \Psi_{\sigma'}(\mathbf{r}') \Psi_\sigma(\mathbf{r}) d^3\mathbf{r} d^3\mathbf{r}' \quad (2.2.17)$$

---

<sup>1</sup>we will also define  $\psi_{ni}(\mathbf{r}) \equiv \psi_\alpha(\mathbf{r} - \mathbf{R}_i)$

We now substitute (2.2.14) into (2.2.16) to retrieve:

$$H = \sum_{\alpha} \sum_{ij} \sum_{\sigma} t_{ij}^{\alpha} c_{\alpha i \sigma}^{\dagger} c_{\alpha j \sigma} + \frac{1}{2} \sum_{\alpha \beta \gamma \delta} \sum_{nmjk} \sum_{\sigma \sigma'} U_{nmjk}^{\alpha \beta \gamma \delta} c_{\alpha n \sigma}^{\dagger} c_{\beta m \sigma'}^{\dagger} c_{\gamma k \sigma'} c_{\delta j \sigma} \quad (2.2.18)$$

where we defined:

$$t_{ij}^{\alpha} = \int \psi_{\alpha i}^{*}(\mathbf{r}) \left[ \frac{\mathbf{p}^2}{2m} + V_I(\mathbf{r}) \right] \psi_{\alpha j}(\mathbf{r}) d^3 \mathbf{r} \quad (2.2.19)$$

and

$$U_{nmjk}^{\alpha \beta \gamma \delta} = \iint \psi_{\alpha n}^{*}(\mathbf{r}) \psi_{\beta m}^{*}(\mathbf{r}') V_{ee}(\mathbf{r} - \mathbf{r}') \psi_{\gamma j}(\mathbf{r}) \psi_{\delta k}(\mathbf{r}') d^3 \mathbf{r} d^3 \mathbf{r}' \quad (2.2.20)$$

We now need to make some simplifying assumptions to get the standard Hubbard model.

Firstly, we assume that the Fermi surface lies within just one conduction band (which can be achieved near absolute zero). This means that to examine interactions near the Fermi energy scale we can ignore all higher energy bands, thus obtaining a narrow-band theory. Moreover, far into the atomic limit we may consider nearest neighbor interactions only and neglect any longer range parameters. Finally, assuming that all sites are equivalent, then we will find that  $t_{ij} \equiv t$  for all nearest neighbors  $\langle ij \rangle$  (the  $t_{ii}$  terms only provide an energy offset and can be safely ignored). Similarly,  $U_{iiii} \equiv U$  giving:

$$\hat{H} = -t \sum_{\langle ij \rangle \sigma} c_{i\sigma}^{\dagger} c_{j\sigma} + \frac{U}{2} \sum_i \sum_{\sigma \sigma'} c_{i\sigma}^{\dagger} c_{i\sigma'}^{\dagger} c_{i\sigma'} c_{i\sigma} + V \sum_{\langle ij \rangle} \sum_{\sigma \sigma'} c_{i\sigma}^{\dagger} c_{j\sigma'}^{\dagger} c_{j\sigma'} c_{i\sigma} \quad (2.2.21)$$

We can make use of the fermion anti-commutation relations:

$$\{c_i, c_j^{\dagger}\} = \delta_{ij}, \quad \{c_i^{\dagger}, c_j^{\dagger}\} = \{c_i, c_j\} = 0 \quad (2.2.22)$$

to find that:

$$\sum_{\sigma \sigma'} c_{i\sigma}^{\dagger} c_{i\sigma'}^{\dagger} c_{i\sigma'} c_{i\sigma} = c_{i\uparrow}^{\dagger} c_{i\downarrow}^{\dagger} c_{i\downarrow} c_{i\uparrow} + c_{i\downarrow}^{\dagger} c_{i\uparrow}^{\dagger} c_{i\uparrow} c_{i\downarrow} = 2n_{i\uparrow} n_{i\downarrow} \quad (2.2.23)$$

and similarly:

$$\sum_{\sigma \sigma'} c_{\sigma i}^{\dagger} c_{\sigma j}^{\dagger} c_{\sigma j} c_{\sigma i} = n_i n_j \quad (2.2.24)$$

Therefore, the Extended Fermi-Hubbard model (EFHM) is governed by the following hamiltonian:

$$H = -t \sum_{\langle ij \rangle \sigma} (c_{i\sigma}^{\dagger} c_{j\sigma} + h.c.) + U \sum_i n_{i\uparrow} n_{i\downarrow} + V \sum_{\langle ij \rangle} n_i n_j \quad (2.2.25)$$

## 2.3 Derivation for bosons

Let us now move our attention to the related problem of modelling an ultracold bose gas loaded on an optical lattice as described in Refs. [22, 23]. The analogy with the FHM is almost immediate. We can view the optical lattice as the replacement of the ionic lattice in the fermion model. The

potential produced by it can be modelled as a sinusoid:

$$V_{lat}(\mathbf{r}) = V_x^2 \sin^2(k_x x) + V_y^2 \sin^2(k_x y) + V_z^2 \sin^2(k_x z) \quad (2.3.1)$$

where  $k_i = \frac{2\pi}{\lambda_i}$  are the wavenumbers of the lasers creating the lattice, and  $V_i$  are their respective amplitudes times the atomic polarizabilities. The lattice spacings are then given by  $a_i = \lambda_i/2$ .

Unfortunately however we no longer have the electron-electron interactions which came naturally when dealing with an electron model, their bosonic counterparts must be made artificially. The Hubbard potential  $U$  can be added by introducing an external trapping potential

$$V_{trap}(\mathbf{r} - \mathbf{r}_i) = g\delta(\mathbf{r} - \mathbf{r}_i) \quad (2.3.2)$$

whose depth determines the interaction strength. The extended Hubbard potential  $V_{ext}$  can instead be achieved by using dressed Rydberg atoms [15] whose dipole-dipole interactions can be made to scale as  $\frac{1}{r^3}$ .

Overall the hamiltonian of a boson gas loaded on such an optical lattice is described well by:

$$H = \int \Psi^\dagger(\mathbf{r}) \left[ \frac{\mathbf{p}^2}{2m} + V_{lat}(\mathbf{r}) \right] \Psi(\mathbf{r}) d^3\mathbf{r} \quad (2.3.3)$$

$$+ \frac{1}{2} \iint \Psi^\dagger(\mathbf{r}) \Psi^\dagger(\mathbf{r}') (V_{trap} + V_{ext})(\mathbf{r} - \mathbf{r}') \Psi(\mathbf{r}') \Psi(\mathbf{r}) d^3\mathbf{r} d^3\mathbf{r}' \quad (2.3.4)$$

The derivation of the Bose-Hubbard model is now nearly identical up until (2.2.21), we just have to ignore the spin indices  $\sigma, \sigma'$  and find:

$$H = -t \sum_{\langle ij \rangle} (c_i^\dagger c_j + h.c.) + \frac{U}{2} \sum_i c_i^\dagger c_i^\dagger c_i c_i + V \sum_{\langle ij \rangle} c_i^\dagger c_j^\dagger c_j c_i \quad (2.3.5)$$

We can make use of the boson commutation relations:

$$[c_i, c_j^\dagger] = \delta_{ij}, \quad [c_i^\dagger, c_j^\dagger] = [c_i, c_j] = 0 \quad (2.3.6)$$

to find that:

$$c_i^\dagger c_i^\dagger c_i c_i = c_i^\dagger (c_i c^\dagger - 1) c_i = n_i(n_1 - 1) \quad (2.3.7)$$

and

$$c_i^\dagger c_j^\dagger c_j c_i = n_i n_j \quad (2.3.8)$$

Therefore, the Extended Bose-Hubbard model (EBHM) is governed by the following hamiltonian:

$$H = -t \sum_{\langle ij \rangle} (c_i^\dagger c_j + h.c.) + \frac{U}{2} \sum_i n_i(n_1 - 1) + V \sum_{\langle ij \rangle} n_i n_j \quad (2.3.9)$$

The origin of the  $\frac{n_i(n_i-1)}{2}$  term in the on-site interaction can also be understood if we consider how many combinations of (unordered) pairs we can make out of  $n_i$  particles on site  $i$ .

## 2.4 Symmetries of the models

Exact diagonalization by itself will not allow us to access system sizes that are sufficiently large, we need a technique to reduce the Hilbert space dimension under consideration. One such numerical technique is block-diagonalisation. We identify a number of conserved quantities our models and use them to diagonalize the Hamiltonian into blocks corresponding to different quantum numbers of these symmetries. The two symmetries that we will often employ in our exact diagonalization are translational and parity symmetry.

### 2.4.1 Translational symmetry

As with most lattice models (where all sites are equivalent), the Hubbard models inherit the symmetries of the lattice they are defined on. It follows that if we impose periodic boundary conditions (PBCs), so that  $i \leftrightarrow i + L$  are interchangeable, then both (2.2.25) and (2.3.9) will have a discrete translational symmetry. To better define this symmetry, let us define the translation operator  $T$

$$T = \prod_i \sigma_{i,i+1} = \sigma_{01}\sigma_{12}\sigma_{23}\dots\sigma_{L-1L} \quad (2.4.1)$$

where  $\sigma_{ij}$  transposes sites  $i$  and  $j$ . This operator simply translates all sites to the right by one so that its action on a Fock state  $|n_0\ n_1\ n_2\dots n_{L-2}\ n_{L-1}\rangle$  (with  $n_i$  particles on site  $i$ ) may be expressed as:

$$T|n_0, n_1, n_2, \dots n_{L-2}, n_{L-1}\rangle = |n_{L-1}, n_1, n_2, \dots n_{L-3}, n_{L-2}\rangle \quad (2.4.2)$$

Then it can be easily verified that the Extended Hubbard models with PBCs are invariant under translation operator  $T$ :

$$T^\dagger HT = H \iff [H, T] = 0 \quad (2.4.3)$$

Since  $H$  and  $T$  commute, they must also be simultaneously diagonalizable. In other words, there exists a basis  $|E, k\rangle$  which block-diagonalizes the Hamiltonian into sectors with different eigenvalues of  $T$ . These eigenvalues are defined to be  $e^{ika}$  where  $a$  is the lattice spacing, and the corresponding eigenvectors are Bloch states:

$$T|k\rangle = e^{ika}|k\rangle, \quad k = \frac{2\pi m}{L}, \quad m \in \mathbb{Z}_L \quad (2.4.4)$$

where the semi-momenta  $k$  are quantized since we must have that  $T^N = 1$ . Given a reference state  $|a\rangle$  in the occupation basis, we can construct a momentum state out of it:

$$|a, k\rangle = \frac{1}{\sqrt{N}} \sum_{m=1}^{L-1} e^{-ikma} T^m |a\rangle \quad (2.4.5)$$

as discussed in Ref. [33]. Indeed:

$$T|a, k\rangle = \frac{1}{\sqrt{N}} \sum_{m=1}^{L-1} e^{-ikma} T^{m+1} |a\rangle = e^{ika} \frac{1}{\sqrt{N}} \sum_{m=1}^{L-1} e^{-ik(m+1)a} T^{m+1} |a\rangle = e^{ika} |a\rangle \quad (2.4.6)$$

as required by (2.4.4).

### 2.4.2 Parity operator

Similarly, we may also define the parity operator  $P$ :

$$P = \prod_i^{\lfloor L/2 \rfloor} \sigma_{i,L-i-1} = \sigma_{0L-1}\sigma_{1L-2}\sigma_{2L-3}\dots\sigma_{\lfloor L/2 \rfloor L-\lfloor L/2 \rfloor-1} \quad (2.4.7)$$

which reflects the chain about its perpendicular bisector. An important property of  $P$  is that it is idempotent i.e.  $P^2 = \mathbb{1}$ . We also define a state satisfying  $P|a\rangle = |a\rangle$  as having positive parity, while  $P|a\rangle = -|a\rangle$  implies negative parity. Finally, we also have that:

$$TP = PT^{-1} \quad (2.4.8)$$

Intuitively, translating a reflected chain to the right is equivalent to translating the chain to the left and then reflecting it. This is exactly what (2.4.8) states.

The extended Hubbard models with OBCs or PBCs are invariant under parity transformations and can both be diagonalized in  $p$  blocks. Following our construction of momentum states, the construction of parity states is fairly trivial:

$$|a,p\rangle = \frac{1}{\sqrt{N}} \sum_{m=1}^{L-1} (1-pP)|a\rangle \quad (2.4.9)$$

Indeed:

$$P|a,p\rangle = \frac{1}{\sqrt{N}} \sum_{m=1}^{L-1} (P-pP^2)|a\rangle = p \frac{1}{\sqrt{N}} \sum_{m=1}^{L-1} (1-pP)|a\rangle = p|a,p\rangle \quad (2.4.10)$$

as desired.

Let us now extend our construction in (2.4.5) to include both translational and parity symmetry:

$$|a,k,p\rangle = \frac{1}{\sqrt{N}} \sum_{m=1}^{L-1} e^{-ikma} T^m (1+pP)|a\rangle \quad (2.4.11)$$

Clearly this is still a momentum state. However, applying the parity operator we see that:

$$P|a,k,p\rangle = \frac{1}{\sqrt{N}} \sum_{m=1}^{L-1} e^{-ikma} T^{-m} (P+pP^2)|a\rangle \quad (2.4.12)$$

$$= p \frac{1}{\sqrt{N}} \sum_{m=1}^{L-1} e^{ikma} T^m (1+pP)|a\rangle = p|a,k,p\rangle \quad (2.4.13)$$

Thus  $|a,k,p\rangle$  is indeed a state with parity  $p = \pm 1$ , provided that  $e^{-ikma} = e^{ikma} \implies kma = 0, \pi$ . The reason we have this constraint is that  $[T, P] \neq 0$ , so we cannot in general have simultaneous eigenstates of both the translation and parity operators. Nevertheless, a lot of the interesting physics in a system can often be probed in the  $k = 0$  and  $k = \pi$  sectors (indeed we will mostly work

in these blocks only), so this shall not be a restrictive constraint.

## 2.5 Exact block-diagonalisation results

We use the translational and parity symmetry to compute the exact energy spectrum of a 1D EBHM chain of length  $L = 12$  at quarter-filling with periodic boundary conditions. All numerical simulations in this work were done using the QuSpin python package [39, 40].

# CHAPTER 3

---

## The Eigenstate Thermalization Hypothesis (ETH)

### 3.1 Introduction

In classical physics we justify the equivalence of statistical ensemble averages with the long time average of an observable via ergodicity. In most cases the non-linear time evolution of phase space trajectories guarantees that a thermal state will be constructed in the infinite time limit as a system covers all of the available phase space. Due to the linearity of Schrodinger's equation, this classical reasoning is not applicable to quantum systems whose thermalization process must therefore be radically different.

First presented by Deutsch in 1991 [7] and Srednicki in 1994 [35–37], the Eigenstate Thermalization Hypothesis (ETH) attempts to solve this issue by requiring that thermalization occur at the level of individual eigenstates, with the dephasing due to time evolution revealing a hidden, already thermal state. Models exhibiting this behaviour are known as thermal or (quantum) ergodic. Of great interest are cases where the ergodicity of a system is broken, with two famous examples being many body localized systems and integrable systems. Equally alluring are a new class of models, known as weak-ergodicity breaking models, which are athermal only in a vanishingly small fraction of the Hilbert space. Recent advances in this topic and the onset of tunable cold-atom experiments have led to flurry of papers investigating such models.

In this chapter we give a general overview on the emergence of ETH and the statements it makes about when and how isolated quantum systems achieve thermal equilibrium, explaining how the ansatz proposed by Srednicki [37] ensures thermalization. Furthermore, we present two bosonic Hubbard models that exhibit signatures of weak ergodicity breaking, and provide numerical results obtained from exact diagonalisation to corroborate our claims. We conclude by identifying two different types of atypical states in our models, those which preserve their lack of ergodicity after a quench, and those which do not. We further identify strong and weak robustness to quenches in the latter category, identifying examples of such states in our models.

## 3.2 Quantum Ensembles

A closed isolated quantum system is well described by the microcanonical ensemble at a fixed energy  $E$  with small uncertainty  $\Delta E$ . The density operator associated to this ensemble is:

$$\hat{\rho}_{MC} = \frac{1}{\mathcal{N}_{E,\Delta E}} \sum_{\substack{n \\ E_n \in I}} |n\rangle \langle n|, \quad I = \left[ E - \frac{\Delta E}{2}, E + \frac{\Delta E}{2} \right] \quad (3.2.1)$$

where  $\hat{H}|n\rangle = E_n|n\rangle$  and  $\mathcal{N}_{E,\Delta E}$  is the number of states in the energy window  $I$ . We should have that the energy expectation value in this ensemble be equal to  $E$ :

$$E = \text{Tr}(\hat{\rho}_{MC}\hat{H}) \equiv \langle H \rangle_{MC} \quad (3.2.2)$$

We can also associate an inverse temperature  $\beta = \frac{1}{T}$  to a closed isolated system by requiring that:

$$E = \text{Tr}(\hat{\rho}_C\hat{H}) \equiv \langle H \rangle_C \quad (3.2.3)$$

where  $\rho_C$  is the canonical ensemble density operator:

$$\hat{\rho}_C = \frac{1}{Z} e^{-\beta\hat{H}}, \quad Z = \text{Tr } e^{-\beta\hat{H}} \quad (3.2.4)$$

Finally, we introduce the diagonal ensemble as discussed in Ref. [31] which, unlike the previous two ensembles, retains memory of the initial state  $|\psi\rangle = \sum_n c_n|n\rangle$  of the system. The motivation behind this ensemble will be explained in the next subsection, but for now we state the result:

$$\hat{\rho}_{DE} = \sum_n |c_n|^2 |n\rangle \langle n| \quad (3.2.5)$$

## 3.3 Thermalization in Quantum systems

Consider a bounded, isolated quantum system with non-degenerate energy eigenvalues  $E_n$  and corresponding eigenstates  $|n\rangle$ . Suppose the system starts out in a superposition of energy states centered at energy  $E$ :

$$|\psi(t)\rangle = \sum_n c_n e^{-iE_n t} |n\rangle \quad (3.3.1)$$

where  $\sum_n |c_n|^2 = 1$ . It is easy to see that given some observable with an associated operator  $\hat{A}$ , its expectation value will evolve as <sup>1</sup>:

$$\langle A(t) \rangle = \langle \psi(t) | \hat{A} | \psi(t) \rangle = \sum_n |c_n|^2 A_{nn} + \sum_{n \neq m} c_m^* c_n e^{-i(E_n - E_m)t} A_{mn} \quad (3.3.2)$$

where we can recognize  $\langle m|A|n\rangle$  as the matrix elements  $A_{mn}$  of operator  $A$  in the energy basis. Physical intuition suggests that the first sum (time independent) will give the value  $\langle A(t) \rangle$  relaxes to, while the second term encodes the time fluctuations in  $\langle A(t) \rangle$  about its equilibrium value.

---

<sup>1</sup>we follow the Schrodinger picture where  $|\psi(t)\rangle = e^{-i\hat{H}t}|\psi\rangle$

Indeed, the infinite time expectation value of  $A$  can be found by averaging  $\langle A(t) \rangle$  over a time interval  $T \rightarrow \infty$ :

$$\overline{\langle A(t) \rangle} \equiv \lim_{T \rightarrow \infty} \frac{1}{T} \int_0^T \langle A(t) \rangle dt = \lim_{T \rightarrow \infty} \frac{1}{T} \langle \psi(t) | \hat{A} | \psi(t) \rangle \quad (3.3.3)$$

$$= \sum_{nm} c_m^* c_n A_{mn} \left( \frac{1}{T} \int_0^T e^{-i(E_n - E_m)t} dt \right) \quad (3.3.4)$$

$$= \sum_n |c_n|^2 A_{nn} + \sum_{m \neq n} c_m^* c_n A_{mn} \left( \frac{1}{T} \int_0^T e^{-i(E_n - E_m)t} dt \right) \quad (3.3.5)$$

For most quantum many-body systems the decoherence should be strong enough to make the second term in (3.3.5) vanish. Hence we find that:

$$\overline{\langle A(t) \rangle} = \sum_n |c_n|^2 A_{nn} \quad (3.3.6)$$

Note however that the definition of the diagonal ensemble implies:

$$\langle A \rangle_{DE} = \sum_n |c_n|^2 A_{nn} = \overline{\langle A(t) \rangle} \quad (3.3.7)$$

We may thus interpret the diagonal ensemble as the long-time averaged ensemble of a system undergoing unitary time evolution.

If we want the system to thermalize then we must require that the prediction by the diagonal ensemble match those made by the microcanonical ensemble:

$$\langle A \rangle_{DE} \stackrel{?}{=} \langle A \rangle_{mc} \iff \sum_n |c_n|^2 A_{nn} \stackrel{?}{=} \frac{1}{\mathcal{N}_{E, \Delta E}} \sum_{\substack{n \\ E_n \in I}} A_{nn} \quad (3.3.8)$$

## 3.4 The Eigenstate Thermalization Hypothesis

The main questions that ETH tries to answer are “when is (3.3.8) true for a given  $\hat{A}$ ?” and “how does  $\langle A(t) \rangle$  approach its equilibrium value when it does?”. As pointed in Ref. [8], this is a fundamental question underpinning the whole field of quantum statistical mechanics.

Firstly, it is paramount to note that the LHS of (3.3.8) retains memory of the system’s initial state via the  $c_n$  coefficients, while the RHS is completely independent of these starting conditions. Thus if thermalization is to occur then we need the matrix elements  $A_{nn}$  to be constant over  $[E - \frac{\Delta E}{2}, E + \frac{\Delta E}{2}]$ , and hence vary smoothly as a function of  $E$  (to leading order):

$$A_{nn} = \mathcal{A}(E) + O(N^{-1}) + O(e^{-S_{th}/2}) \quad (3.4.1)$$

as stated in Ref. [37].

Physically this means that every eigenstate should be able thermalize so that no matter what initial conditions the system starts out in, it will reach equilibrium. This is distinctly different from the

classical process of thermalization which hinges on the time evolution of a system allowing it to explore the entire available phase space.

Following [37] we should also ensure that the averaged temporal fluctuations of  $\langle A(t) \rangle$  about  $\langle A \rangle_{DE}$  be exponentially small. We find that

$$\overline{(\langle A(t) \rangle - \langle A \rangle_{DE})^2} = \lim_{T \rightarrow \infty} \frac{1}{T} \int_0^T (\langle A(t) \rangle - \langle A \rangle_{DE})^2 dt \quad (3.4.2)$$

$$= \lim_{T \rightarrow \infty} \frac{1}{T} \int_0^T \left( \sum_{m \neq n} c_m^* c_n e^{-i(E_n - E_m)t} A_{mn} \right)^2 dt \quad (3.4.3)$$

$$= \sum_{m \neq n} |c_m|^2 |c_n|^2 |A_{mn}|^2 \quad (3.4.4)$$

$$+ \lim_{T \rightarrow \infty} \frac{1}{T} \int_0^T \left( \sum_{\{m,n,\alpha,\beta\}} c_m^* c_n c_\alpha^* c_\beta e^{-i(E_n + E_\beta - E_m - E_\alpha)t} A_{mn} A_{\alpha\beta} \right) dt \quad (3.4.5)$$

where  $\{m, n, \alpha, \beta\} = m \neq n, \alpha \neq \beta, \alpha \neq n, \beta \neq m$ . Again the dephasing should be strong enough to make the second integral vanish, giving us the following result

$$\overline{(\langle A(t) \rangle - \langle A \rangle_{DE})^2} = \sum_{m \neq n} |c_m|^2 |c_n|^2 |A_{mn}|^2 \quad (3.4.6)$$

Since the  $c_i$  coefficients are normalized to unity we find using the triangle inequality:

$$\overline{(\langle A(t) \rangle - \langle A \rangle_{DE})^2} \leq \max |A_{mn}|^2 \sim e^{-S_{th}(\bar{E})} \implies A_{mn} \sim e^{-S_{th}(\bar{E})/2} \quad (3.4.7)$$

Consequently, assuming the off diagonal elements of  $A$  are small enough, the deviation of  $\langle A(t) \rangle$  from its equilibrium value averages to an exponentially small value dictated by the density of states in the chosen energy window.

One class of models which are known to satisfy (3.4.1) and (3.4.7) are known as quantum chaotic systems [5, 14], whose matrix elements satisfy:

$$A_{mn} = \bar{A} \delta_{mn} + \sqrt{\frac{\bar{A}^2}{d}} R_{mn} \quad (3.4.8)$$

where  $d$  is the Hilbert space dimension,  $\bar{A} = \frac{1}{d} \sum_i A_{ii}$ ,  $R_{mn}$  is a random value taken from a gaussian distribution of zero mean and variance  $\sigma = 1$ . However, there are some problems with this ansatz. First of all, it assumes that the diagonal elements of the matrix do not vary significantly along the entire Hilbert space. Furthermore, the off-diagonal elements experience no exponential suppression by the density of states.

Eq. (3.4.8) can be generalized allowing us to express ETH as it was written down by Srednicki in 1999 [37]:

$$A_{nm} = \mathcal{A}(\bar{E}) \delta_{nm} + e^{-S_{th}(\bar{E})/2} R_{nm} f(\omega, \bar{E}) \quad (3.4.9)$$

Here  $\omega = \frac{E_n - E_m}{2}$  is the energy difference,  $\bar{E} = \frac{E_n + E_m}{2}$  is the average energy,  $S_{th}(\bar{E})$  is the thermodynamic entropy at energy  $\bar{E}$ ,  $R_{nm}$  is a random number from a normal distribution and

$\mathcal{A}(\bar{E}) \equiv \langle A \rangle_{mc}$ ,  $f(\omega, \bar{E})$  are smooth functions of their arguments. Note that taking the limit of (3.4.9) in a very small energy window known as Thouless energy window, then we get (3.4.8) back as expected [5, 37].

### 3.5 Important remarks on ETH

Firstly note that the full statement of ETH allows us to describe in mathematical terms what we mean by “small” when describing  $\Delta E$ . Indeed using (3.4.9) we find that:

$$\overline{\langle A(t) \rangle} = \sum_n |c_n|^2 \mathcal{A}(E_n) + O(e^{-S_{th}/2}) \quad (3.5.1)$$

Following [36] we can expand  $\mathcal{A}(E_n)$  as a taylor series about  $E$ :

$$\mathcal{A}(E_n) = \mathcal{A}(E) + (E_n - E)\mathcal{A}'(E) + \frac{1}{2}(E_n - E)^2\mathcal{A}''(E) + \dots \quad (3.5.2)$$

and substitute into (3.5.1) to find:

$$\overline{\langle A(t) \rangle} = \mathcal{A}(E) + \frac{1}{2} \sum_n |c_n|^2 (E_n - E)^2 \mathcal{A}''(E) + o(e^{-S_{th}/2}) \quad (3.5.3)$$

$$= \mathcal{A}(E) + \frac{1}{2} (\Delta E)^2 \mathcal{A}''(E) + o(e^{-S_{th}/2}) \quad (3.5.4)$$

where to get to the last line we used

$$(\Delta E)^2 = \sum_n |c_n|^2 (E_n - E)^2 \quad (3.5.5)$$

If we want (3.5.4) to replicate the microcanonical average  $\mathcal{A}(E)$  then we must require that:

$$(\Delta E)^2 \left| \frac{\mathcal{A}''(E)}{\mathcal{A}(E)} \right| \ll 1 \quad (3.5.6)$$

Assuming the above is satisfied then we do indeed find that:

$$\overline{\langle A(t) \rangle} = \mathcal{A}(E) + O(\Delta E^2) \quad (3.5.7)$$

Another remarkable consequence of (3.3.8) is the equivalence of statistical ensembles. Indeed, noting that the microcanonical and canonical ensembles are related to each other through a Laplace transform, if we let  $|c_n|^2 = \frac{1}{Z} e^{-\beta E_n}$  then we find that the microcanonical prediction will be equal to the canonical prediction.

We should also note that the fluctuations derived in (3.4.7) are not thermal fluctuations predicted by statistical mechanics as they are too small. Let us instead look at what would normally be referred to as the quantum mechanical uncertainty:

$$(\Delta A(t))^2 = \langle A^2(t) \rangle - \langle A(t) \rangle^2 \quad (3.5.8)$$

It is easy to see that provided there are no degeneracies then:

$$\overline{\langle A(t) \rangle^2} = \langle A \rangle_{DE}^2 \stackrel{ETH}{=} \langle A \rangle_{MC}^2 \quad (3.5.9)$$

Also, it can be shown [36] that the structure of (3.4.9) is preserved under matrix multiplication:

$$(A^2)_{nm} = \mathcal{A}'(\bar{E})\delta_{nm} + e^{-S'_{th}(\bar{E})/2}R'_{nm}f'(\omega, \bar{E}) \quad (3.5.10)$$

This yields

$$\overline{\langle A^2(t) \rangle} \stackrel{ETH}{=} \langle A^2 \rangle_{MC} \quad (3.5.11)$$

$$\implies \overline{\langle A^2(t) \rangle - \langle A(t) \rangle^2} = \langle A^2 \rangle_{MC} - \langle A \rangle_{MC}^2 + O(N^{-1}) + O(e^{-S/2}) + O(\Delta E^2) \quad (3.5.12)$$

so the time averaged quantum fluctuations reproduce the thermal fluctuations expected by the microcanonical ensemble.

We have thus far neglected one important question in our discussion of ETH, namely the dynamics leading to thermalization. Indeed the states described by (3.2.1) and (3.2.4) are clearly mixed, so how could a pure state  $|\psi\rangle$  evolve into a thermally mixed state? The answer is that in general no system can globally thermalize <sup>2</sup> as a result of conservation of information (in this case information on the system's initial state). However, it is still possible to have the information get scrambled across the system leading to non-local information conservation and thus local thermalization.

Motivated by this we consider a small subsystem  $S$  surrounded by the rest of the system  $\bar{S}$ . The reduced density matrix  $\rho_S = \text{Tr}_{\bar{S}}(|\psi\rangle\langle\psi|)$  will be a mixed state and could hypothetically evolve into a thermal ensemble with  $\bar{S}$  acting as a heat reservoir for  $S$ . The dynamics behind thermalization would then be driven by the interactions of  $S$  with the rest of the system: as  $S$  gets more and more entangled with  $\bar{S}$  eventually we will reach thermal equilibrium, and the entanglement entropy  $S_S = -\text{Tr}(\rho_S \ln \rho_S)$  will be maximized to the thermal entropy  $S_{th} = -\text{Tr}(\rho_{MC} \ln \rho_{MC})$ . Consequently if subsystem  $S$  has reached equilibrium then we should expect its entanglement entropy to follow a volume scaling law due to its equivalence with the extensive thermal entropy.

Another aspect of ETH that hasn't been clarified sufficiently is the type of operators that should be considered [11]. In general it is assumed that only local operators, such as the occupation of two nearest neighbor sites, should be used. Many global operators, especially those exploiting symmetries of the system, will trivially fail.

It is also important to distinguish between two different forms of ETH. One version, known as weak ETH, posits that only a vanishingly small fraction (in the thermodynamic limit) of eigenstate violate ETH. Strong ETH on the other hand requires all eigenstates to satisfy ETH in the thermodynamic limit.

---

<sup>2</sup>thermalize in the sense that the state evolves into  $\rho_{MC}$

### 3.6 The Quintessential chaotic Bose-Hubbard model

We begin by considering a 1D chain of hard-core bosons with periodic boundary conditions described by the following Hamiltonian [26]:

$$H = -t \sum_i (c_i^\dagger c_{i+1} + h.c.) + V \sum_i n_i n_{i+1} - t' \sum_i (c_i^\dagger c_{i+2} + h.c.) + V' \sum_i n_i n_{i+2} \quad (3.6.1)$$

We set the filling to be  $N = \frac{L}{2}$  and plot the expectation values of  $\frac{1}{L} \sum_i n_i n_{i+1}$  and  $\frac{1}{L} \sum_i (c_i^\dagger c_{i+1} + h.c.)$  for all the eigenstates of (3.6.1) in the  $k = 0$  sector against their respective energies. Due to the translational invariance of our model, these operators yield the same expectation values as  $n_i n_{i+1}$  and  $(c_i^\dagger c_{i+1} + h.c.)$  for any given site  $i$ . According to ETH we should expect to find bands getting narrower as we increase the system size.

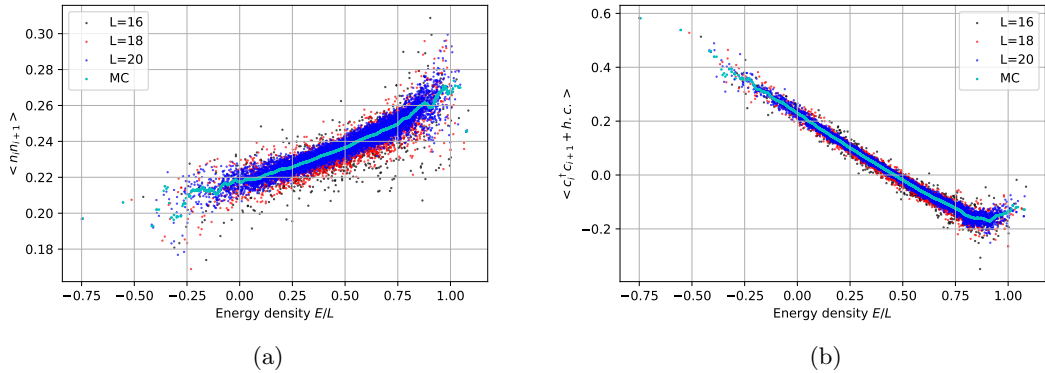


**Figure 3.1.** Eigenstate expectation value (EEV) plots for (a)  $n_i n_{i+1}$  and (b)  $c_i^\dagger c_{i+1} + h.c.$ . Both plots show quintessential thermal behaviour, with small changes in energy only yielding correspondingly small changes in the EEV. We considered three system sizes  $L = 16, 18, 20$ , and let  $t = V = t' = V' = 1$ .

We see that this is precisely what happens for the model in (3.6.1).

### 3.7 Ergodicity breaking: a general overview

As previously mentioned cases where ETH is broken have also gathered a lot of interest recently, and will be the subject of the rest of this work.

There are two well-known classes of models which break ETH strongly. One of these are integrable systems whose extensive number of conservation laws prevents thermalization. In such systems expectation values equilibrate to a generalized Gibbs ensemble. This property of integrability, however, is very sensitive to weak perturbations which can easily re-establish ergodicity. Many-body localized (MBL) systems [1] are another celebrated example of strong ergodicity breaking. Such systems also have a macroscopic number of conserved quantities, but unlike integrable systems one can perturb MBL systems without destroying their athermality, since the effect of local perturbations remains confined.

Furthermore, there are several known processes for which ETH is weakly broken [30]. These include quantum many body scars [30, 38] in the PXP model, confinement in a quantum Ising chain [24, 32] and projector embedding [34].

Interest in quantum many body scars first arose in 2018 when an experiment [2] on a chain of 51 Rydberg atoms in the strong blockade regime revealed persistent oscillations in its domain wall density for certain initial states. These results were reinforced by numerical studies of the PXP model, an effective Hamiltonian which accurately models the dynamics in the Rydberg experiment. This model exhibited periodic fidelity revivals after a quench from a Neel-like product state. These atypical states were also shown to have a sub-thermal entanglement entropy which scaled with the area of the system rather than its volume. Due to their resemblance to scarring in stadium-shaped billiard models, where the path of a wave-packet with certain initial conditions tends to cluster around unstable orbits, the atypical states have taken the name of quantum scars. Several other signatures of athermalization have also been presented since then establishing quantum many body scars as a staple of weak ergodicity breaking. Theories with confinement are also believed to present rare states. Indeed, it has been shown [24, 32] that in both lattice and continuum quantum ising models, the presence of a longitudinal field can induce athermal behaviour due to confinement. More specifically, the longitudinal field generates a linear potential between any two domain walls. These confined domain walls, known as meson excitations, formed a band separate to the continuum when probing the expectation value of a local operator, far away (by at least a standard deviation) from the microcanonical prediction. Numerical and analytical results also showed that these meson excitations persisted after a quench and could influence the short-time non-equilibrium dynamics of the model. Finally, on a more abstract level one can artificially embed rare states into a Hamiltonian’s spectrum via the process of “projector embedding”, introduced by Shiraishi et al. [34]. By choosing projectors satisfying appropriate commutation rules, one can embed specific states into a system’s spectrum.

## 3.8 One-chain model

### 3.8.1 The model

We now consider an extended Bose-Hubbard chain with attractive onsite potential  $U = -4t$ , repulsive intersite potential  $V = 2t$  and with the hopping amplitude  $t = 1$  setting the energy scale. The chain has periodic boundary conditions and is set at quarter filling  $N = \frac{L}{2}$  (thus only even chain lengths are allowed). Due to the PBCs we can diagonalize the Hamiltonian in momentum blocks, in our case we will be interested in the  $k = 0$  block.

### 3.8.2 Absence of integrability

We must firstly make sure that our model is non-integrable. We can do so by looking at the statistical properties of the energy levels and comparing them with predicted values for random matrices.

The use of random matrix theory to study the properties of many body systems was first introduced by Wigner [41–43] in the 1950s in the study of nuclear energy levels and was later refined by Dyson [9]. In his papers, Wigner reasoned that obtaining the exact form of highly excited energy levels is a

hopeless task, and that it is instead far more compelling to look at the spacing between these levels. Arguing that over a sufficiently narrow energy window (where the density of states is more or less constant) the hamiltonian should look approximately random, Wigner showed that the energy level differences  $r$  in a heavy nucleus followed what is now known as the Wigner surmise or Wigner-Dyson distribution:

$$P(r) = \frac{r}{2\sigma^2} e^{-\frac{r^2}{4\sigma^2}} \quad (3.8.1)$$

To see where (3.8.1) comes from, let us consider a  $2 \times 2$  random matrix:

$$H = \begin{pmatrix} \epsilon_1 & \frac{V}{\sqrt{2}} \\ \frac{V^*}{\sqrt{2}} & \epsilon_2 \end{pmatrix} \quad (3.8.2)$$

where  $\epsilon_1, \epsilon_2, V$  are taken from a random Gaussian distribution with zero mean and variance  $\sigma$ . This matrix can be easily diagonalized, giving two energy levels:

$$E_{1,2} = \frac{\epsilon_1 + \epsilon_2 \pm \sqrt{(\epsilon_1 - \epsilon_2)^2 + 2|V|^2}}{2} \quad (3.8.3)$$

Note that if the system has time-reversal symmetry, then the Hamiltonian is a real symmetric matrix and thus  $V = V^*$ . Letting  $r = E_2 - E_1$  be the level spacing, and recalling that the probability distribution of  $\epsilon_1, \epsilon_2, V$  is gaussian:

$$\rho(\epsilon_1, \epsilon_2, V) = \frac{1}{(2\pi)^{3/2}\sigma^3} \exp\left(-\frac{\epsilon_1^2 + \epsilon_2^2 + V^2}{2\sigma^2}\right) \quad (3.8.4)$$

then the spacing distribution is a triple integral:

$$P(r) = \frac{1}{(2\pi)^{3/2}\sigma^3} \iiint \delta(\sqrt{(\epsilon_1 - \epsilon_2)^2 + 2V^2} - r) \exp\left(-\frac{\epsilon_1^2 + \epsilon_2^2 + V^2}{2\sigma^2}\right) d\epsilon_1 d\epsilon_2 dV \quad (3.8.5)$$

This integral in its present form is quite difficult to evaluate due to the argument in the delta function. Following [5] we can perform a change of coordinates  $\epsilon_2 = \epsilon_1 + \sqrt{2}\eta$  which will decouple  $\epsilon_1$  from the delta function and allow us to evaluate a gaussian integral in  $\epsilon_1$ :

$$P(r) = \frac{1}{(2\pi)^{3/2}\sigma^3} \iiint \delta(\sqrt{2}\sqrt{\eta^2 + V^2} - r) \exp\left(-\frac{2\epsilon_1^2 + 2\eta^2 + 2\sqrt{2}\epsilon_1\eta + V^2}{2\sigma^2}\right) d\epsilon_1 \sqrt{2}d\eta dV \quad (3.8.6)$$

$$= \frac{1}{2\pi\sigma^2} \iint \delta(\sqrt{2}\sqrt{\eta^2 + V^2} - r) \exp\left(-\frac{\eta^2 + V^2}{2\sigma^2}\right) d\eta dV \quad (3.8.7)$$

The remaining integral can be evaluated in cylindrical coordinates:  $\eta = R \cos \theta$  and  $V = R \sin \theta$

$$P(r) = \frac{1}{2\pi\sigma^2} \int \delta(\sqrt{2}R - r) \exp\left(-\frac{R^2}{2\sigma^2}\right) R dR d\theta \quad (3.8.8)$$

$$= \frac{1}{2\pi\sigma^2} \int \frac{1}{\sqrt{2}} \frac{r}{\sqrt{2}} \exp\left(-\frac{r^2}{4\sigma^2}\right) d\theta = \frac{r}{2\sigma^2} e^{-\frac{r^2}{4\sigma^2}} \quad (3.8.9)$$

as stated earlier. The numerical calculations show that this distribution applies well to larger

matrices [14] as long as the edges of the spectrum are excluded (these edge states remain localized [5]). Also, a similar calculation for a hamiltonian without time-reversal symmetry shows that:

$$P(r) = \frac{r^2}{2\sqrt{\pi}\sigma^3} e^{-\frac{r^2}{4\sigma^2}} \quad (3.8.10)$$

The ensemble of matrices satisfying (3.8.1) is known as the Gaussian Orthogonal Ensemble (GOE), while those satisfying (3.8.10) form the Gaussian Unitary Ensemble (GOE).

Due to the time-reversal symmetry of our model we should expect to find level statistics similar to the GOE. Indeed, a study [27] of the level spacing in similar extended Bose-Hubbard models has shown that this is indeed the case for sensible Hubbard potential to hopping strength ratios. As explained in Ref. [26] we should only consider a portion of the spectrum with slowly varying density of states (DOS) as the off-diagonal matrix elements induce fluctuations that fall off as the inverse root of the DOS. Looking at fig. 3.2a we see that the density of states is more or less constant (changes at most by a factor of 1.25) for eigenstates between  $\frac{D}{3} = 1846$  and  $\frac{4D}{5} = 4430$ . The lower 33% and the upper 20% of the spectrum can thus be discarded in our level spacing analysis.

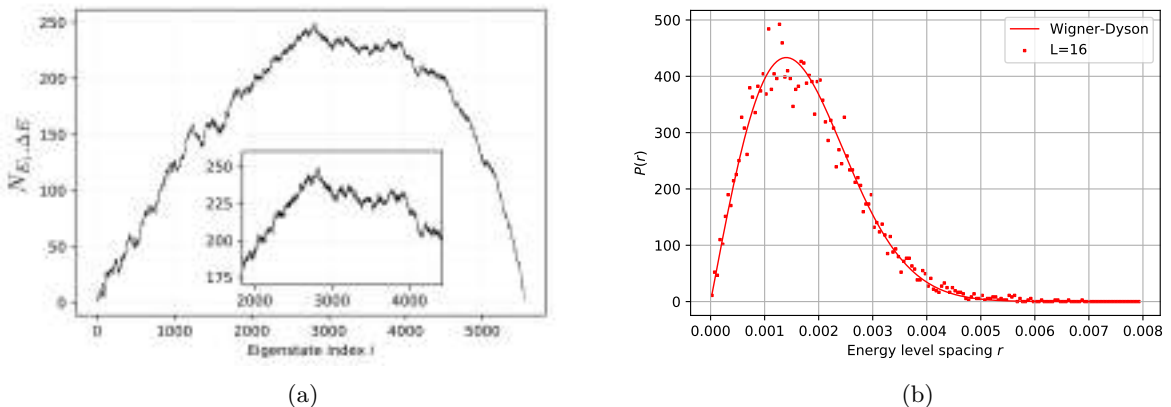


**Figure 3.2.** (a) We plot the number of states  $N_{E_i, \Delta E}$  with energy within the window  $[E_i - \Delta E/2, E_i + \Delta E/2]$  where  $\Delta E = 0.48$  and  $L = 14$  in the  $k = 0$  block. We see that the density of states is slowly varying for  $D/3 < i < 4D/5$ . (b) shows that the energy level statistics follow a Wigner-Dyson distribution (3.8.1).

The energy eigenvalues within the restricted spectrum are sorted in ascending order (i.e.  $E_1 < E_2 < E_3 < \dots$ ) after which we compute the (unfolded) level spacings:

$$r_n = E_{n+1} - E_n \quad (3.8.11)$$

The level spacing plot fig. 3.2b clearly shows that  $P(r)$  is well described by Wigner-Dyson distribution. We may conclude that our model is non-integrable. It is also helpful to plot the expectation value spacing for our operator  $\hat{A} = \frac{1}{L} \sum_i n_i n_{i+1}$  defined as:

$$d_m = \langle m+1 | \hat{A} | m+1 \rangle - \langle m | \hat{A} | m \rangle \quad (3.8.12)$$

as was done in Ref. [26].

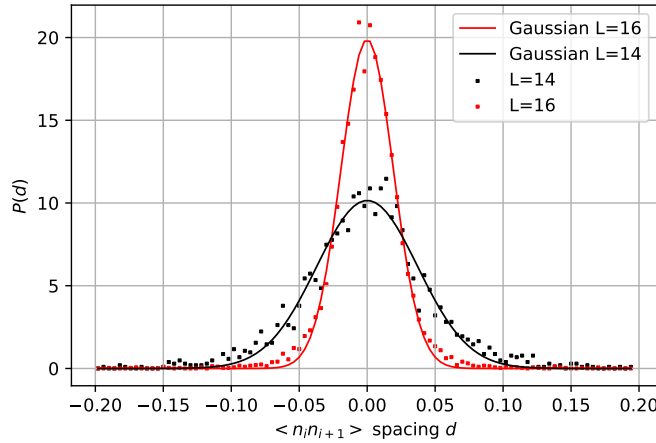


**Figure 3.3.** Expectation value spacing statistics for  $\hat{n}_i \hat{n}_{i+1}$ . Note that the distribution, which is well described by a gaussian, gets narrower as we increase the system size. In the thermodynamic limit it should thus approach a delta function.

We see that  $P(d)$  is well described by a gaussian distribution whose standard deviation decreases with system size. In the thermodynamic limit one should thus expect to obtain a delta function. For a system satisfying (3.4.9) we expect the the expectation value of any local operator (ignoring special cases exploiting symmetries of the model) to be a smooth function of the energy. Thus the spacing between expectation values with consecutive energies must be a vanishingly small quantity, thus producing a delta function centered at zero for large  $L$ . *Kim et al.* also found similar results for their non-integrable, quantum chaotic models.

### 3.8.3 Eigenstate expectation value (EEV) plots

According to ETH, if a system is to thermalize then any local operator's expectation value in the energy eigenstate  $|E\rangle$  should behave as a smooth function of the energy  $E$ . Due to finite size effects what we will get is a smooth band rather than a line, but this band should get narrower as we increase the system size.

We thus plot  $\langle E|n_i n_{i+1}|E\rangle$ ,  $\langle E|n_i^2|E\rangle$ ,  $\langle E|(c_i^\dagger c_{i+1} + h.c.)|E\rangle$  as a function of  $E$  for different system sizes, and check whether this is a smooth, converging (with system size) band or not. To avoid having to project the states out of their symmetry sector we actually average these operators over the chain i.e. evaluate  $\frac{1}{L} \sum_i n_i n_{i+1}$ ,  $\frac{1}{L} \sum_i n_i^2$  and  $\frac{1}{L} \sum_i (c_i^\dagger c_{i+1} + h.c.)$  which due to the translational invariance of our model will be guaranteed to give the same value as the original localized operators.

In fig. 3.4 we see that there is indeed a continuum of states with  $\frac{E}{L} > -1$  that varies smoothly with the energy density, and which seems to tighten as we increase  $L$ . However, there are also several “atypical” states scattered around the plot which have an anomalous EEV which hint at a possible breakdown of ETH. Indeed these abnormal states imply that depending on their initial conditions, two fine-tuned systems starting out in the same energy window can thermalize to different values by retaining memory of their initial state.

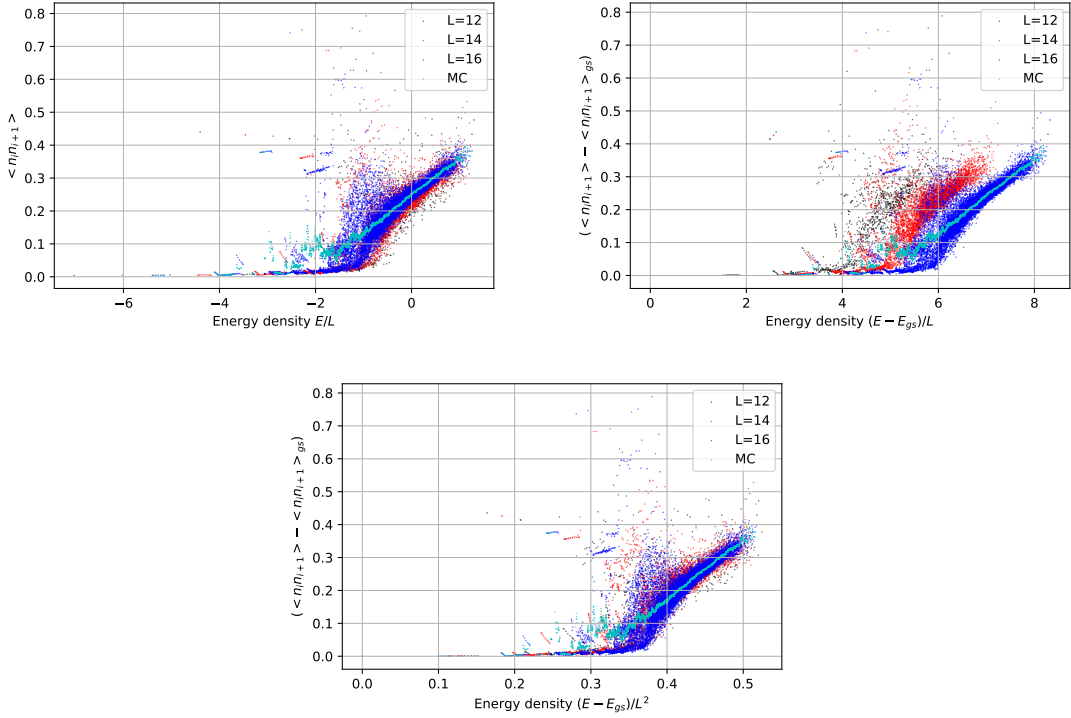


**Figure 3.4.** Eigenstate expectation value (EEV) plots for  $L = 12, 14, 16$  in the  $k = 0$  sector (and  $p = 1$  for  $L = 16$ ). The microcanonical average was computed for  $L = 16$  using a spacing of  $\frac{\Delta E}{L} = 0.03$ . We scale the  $x$ -axis in different ways to reveal the differences in the scaling properties between the low lying and the highly excited states.

In Ref. [32] the energy density and EEVs were also scaled relative to the ground state. This revealed that the atypical states in their confined quantum Ising chain exhibited well-converged atypical states, with a continuum band that also ‘‘qualitatively converged’’. It is evident that in our case there seems to be no such convergence in a quantitative sense. However, a rough convergence of the continuum band can be achieved if we instead plot  $(E - E_{gs})/L^2$  rather than  $(E - E_{gs})/L$  on the  $x$ -axis. This follows from the scaling properties of the bands in our spectrum. Indeed the ground state of our model will have approximately all bosons occupying one site, giving an energy  $E_{GS} \approx -tL(\frac{L}{2} - 1)$ . The low-lying states will have almost all bosons on one site, with a small number  $a$  being displaced on either a far away site, or a nearest neighbor site. In the first case the energy is  $E_{low,1} \approx -t[(L-a)(L-a-2) + a(a-1)]$  while for the second it is  $E_{low,2} \approx -t[(L-a)(L-a-2) + a(a-1)] + V\frac{a^2}{4}$ . Their energy relative to the ground state scales linearly with  $L$ , thus explaining why they almost overlap when scaling by  $L$ . Highly excited states on the other hand will contain very few quadratic terms (as they contribute a lot to reducing the energy) so their relative energy will scale quadratically with  $L$ . This explains why the continuum overlaps when we scale by  $L^2$ .

The scaling of the energies is also clearly shown in following EEV plots for the hopping and hubbard terms of the hamiltonian:

As can be seen from fig. 3.5 the low lying bands mostly vary in energy due to hopping. As we

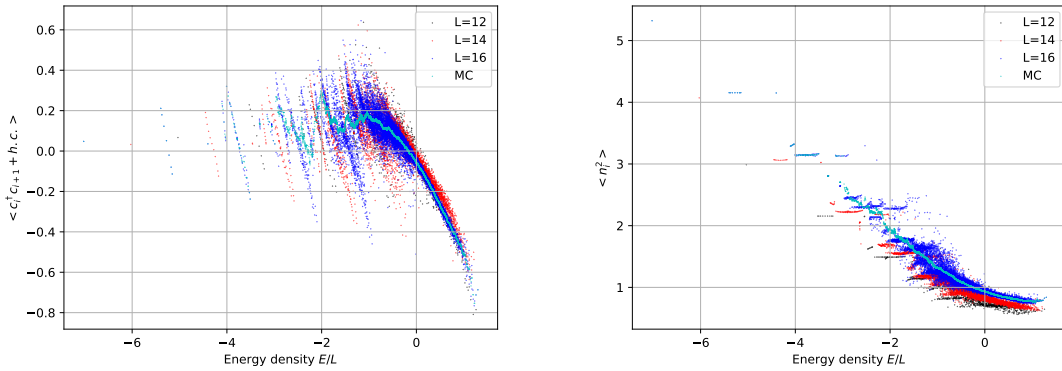


**Figure 3.5.** EEV plots for  $\langle c_i^\dagger c_{i+1} + h.c. \rangle$  and  $\langle n_i^2 \rangle$ , for  $L = 12, 14, 16$ . The microcanonical average was computed for  $L = 16$  using a spacing of  $\frac{\Delta E}{L} = 0.03$ .

increase the energy the Hubbard term gets smaller and smaller, corresponding to less clumping on few sites, leading to the quadratic scaling getting washed out.

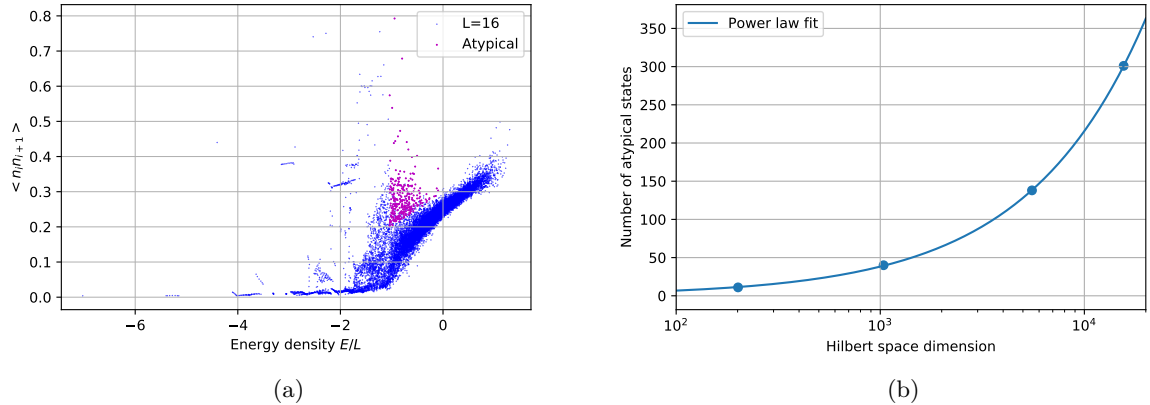


**Figure 3.6.** (a) The atypical states with energies overlapping the continuum ( $\frac{E}{L} > -1$ ) are shown in magenta. These are the states more likely to break ETH. (b) The number of atypical states scales following a power law  $0.21 \times \mathcal{D}^{0.75}$ , where  $\mathcal{D}$  is the Hilbert space dimension  $\mathcal{D}$ .

We also perform in fig. 3.6b a finite size scaling analysis to determine the persistence of the atypical states in the thermodynamic limit. We look at the number of atypical states with energies overlapping with those in the continuum i.e.  $\frac{E}{L} > -1$ . The data is well described by a power law scaling:  $0.21 \times \mathcal{D}^{0.75}$  where  $\mathcal{D}$  is the Hilbert space size. However, the exponential increase of the Hilbert space dimension will quickly suppress this power law scaling. Consequently only a vanishingly small portion of the spectrum violates ETH and thermalization will generally occur without fine tuning of the initial conditions.

### 3.8.4 Off-diagonal matrix elements

We should also check if the off-diagonal elements of our operators in the energy eigenbasis are indeed small enough, and whether or not there is any structure to them. To do so we project

matrix representation  $A$  of the operator  $n_i n_{i+1}$  in the occupation basis to the energy basis:

$$A' = Q A Q^\dagger \quad (3.8.13)$$

where  $Q$  is the change of basis matrix whose column vectors are the energy eigenstates expressed in the fock basis.

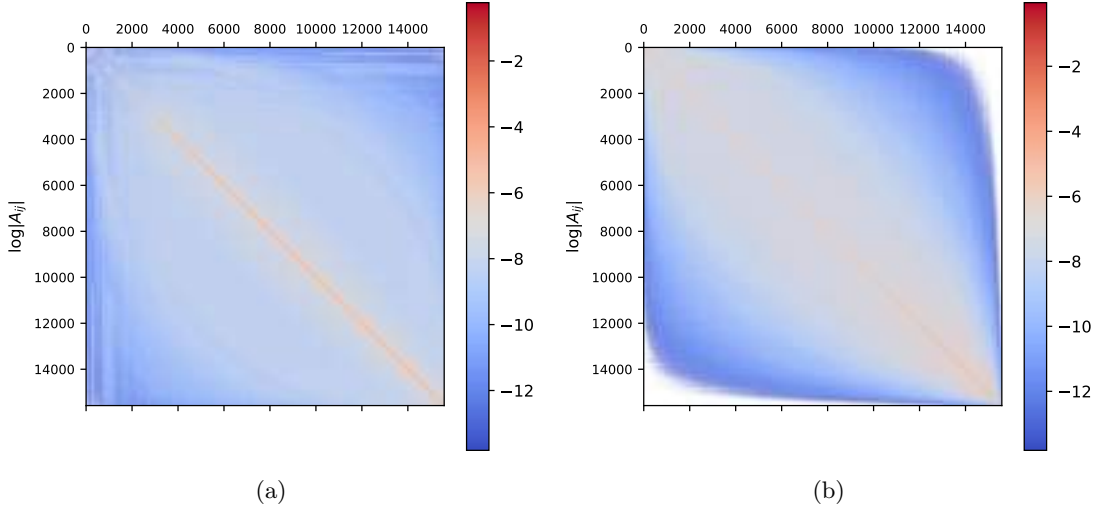


**Figure 3.7.** (a) Natural logarithm of the matrix elements of  $n_i n_{i+1}$  in the energy eigenbasis for  $U = -4t$ . (b) Natural logarithm of the matrix elements of  $n_i n_{i+1}$  in the energy eigenbasis for  $U = 4t$  (which exhibits no atypical states).

As required by ETH the off-diagonal elements are considerably smaller than the diagonal elements. There also seem to be several light lines (and by symmetry rows) which are weakly coupled to the rest of the Hilbert space. However, this structure seems to be inherent to the Hamiltonian itself and persists as we vary  $U$  to be in the range where there are no atypical states. Consequently there is no signature of atypicality in the matrix elements as presented in fig. 3.7a.

### 3.8.5 Time evolution and Quenches

The EEV plots in fig. 3.4 and fig. 3.5 show that there is indeed a class of states which fails to thermalize in the infinite time limit (DE ensemble). This however provides no details on the out-of-equilibrium dynamics at short and intermediate times.

To probe the real time dynamics of our model we consider a narrow energy window  $I$  as shown in fig. 3.8a and take a sample  $S_1$  of atypical states and a sample  $S_2$  of typical states within this window. We then construct two random initial states:

$$|\psi_{typ}\rangle = \sum_{i \in S_1} b_i |E\rangle_i \quad (3.8.14)$$

$$|\psi_{atyp}\rangle = \sum_{i \in S_2} c_i |E\rangle_i \quad (3.8.15)$$

where  $b_i, c_i$  are randomly generated and properly normalized  $\sum_i |b_i|^2 = \sum_i |c_i|^2 = 1$ . These states are then time evolved in the Schrodinger picture by acting the unitary time evolution operator  $\hat{U} = e^{-i\hat{H}t/\hbar}$  on them producing:

$$|\psi_{typ}(t)\rangle = \sum_{i \in S_1} b_i e^{iE_i t} |E\rangle_i \quad (3.8.16)$$

$$|\psi_{atyp}(t)\rangle = \sum_{i \in S_2} c_i e^{iE_i t} |E\rangle_i \quad (3.8.17)$$

Finally, we evaluate the expectation value  $\langle n_i(t) n_{i+1}(t) \rangle$  in these two states.

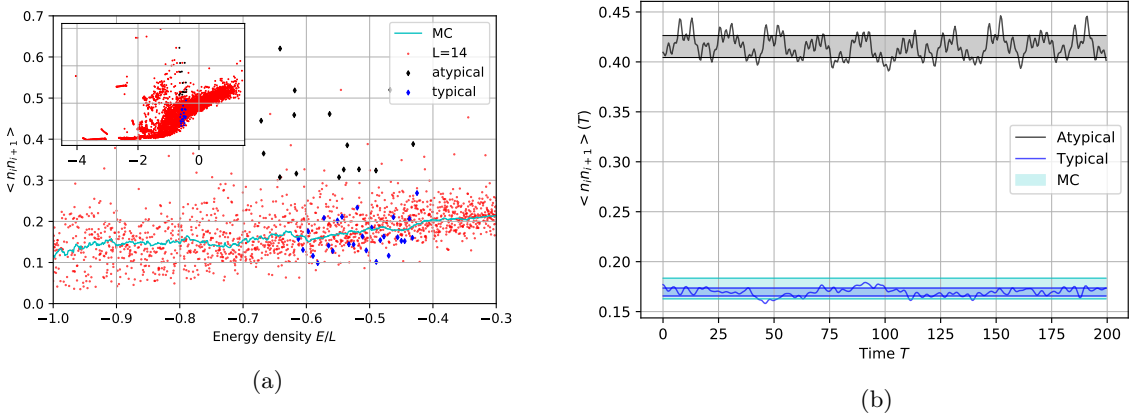


**Figure 3.8.** (a) Sample of typical (blue) and atypical (black) states used to produce the initial states evolved in fig. 3.8b. (b) Time evolution of the superposition of states shown in fig. 3.8a shows that relaxation is quickly achieved for both states in (3.8.16) and (3.8.17) but to different values despite being in the same energy window.

fig. 3.8a shows that both states in (3.8.16) and (3.8.17) relax very quickly to an equilibrium value dictated by their DEs. Despite being in the same energy window, these states relax to different values, further supporting the hypothesis that ETH has been broken. We also computed the standard deviation of the microcanonical prediction in the chosen energy window, and shaded in cyan a confidence interval extending one standard deviation above and below the microcanonical average. We do the same with the temporal fluctuations of the atypical and typical states. We can clearly see that the typical state's fluctuations almost always remains within a standard deviation of the microcanonical average, while the atypical state's fluctuations are several standard deviations away. The athermal behaviour in our model can thus be probed at short times as well.

We can also look at the evolution of  $\langle A \rangle$  after a quench. In a similar fashion to the analysis in Ref. [32], we take the eigenstates of our hamiltonian  $H$  with  $V = 2$  and at time  $t = 0$  perturb the system by quenching the nearest neighbor potential to  $V = 2.2$ :

$$H_i(V = 2) \mapsto H_f(V = 2.2) \quad (3.8.18)$$

In the long time limit the DE predicts[32] that for a given energy eigenstate  $|E_m\rangle$  of  $H_i$  the quenched

expectation values average in the infinite time limit to:

$$\lim_{\tau \rightarrow \infty} \int_0^\tau c_m^* c_n \langle E_m | e^{iHt} A e^{-iHt} | E_m \rangle dt = \sum_n |\tilde{c}_{mn}|^2 \langle \tilde{E}_n | A | \tilde{E}_n \rangle \quad (3.8.19)$$

where  $\tilde{E}_n$  are the eigenstates of  $H_f$  and  $\tilde{c}_{mn} = \langle E_m | \tilde{E}_n \rangle$ . The results for this quench are shown in fig. 3.9.

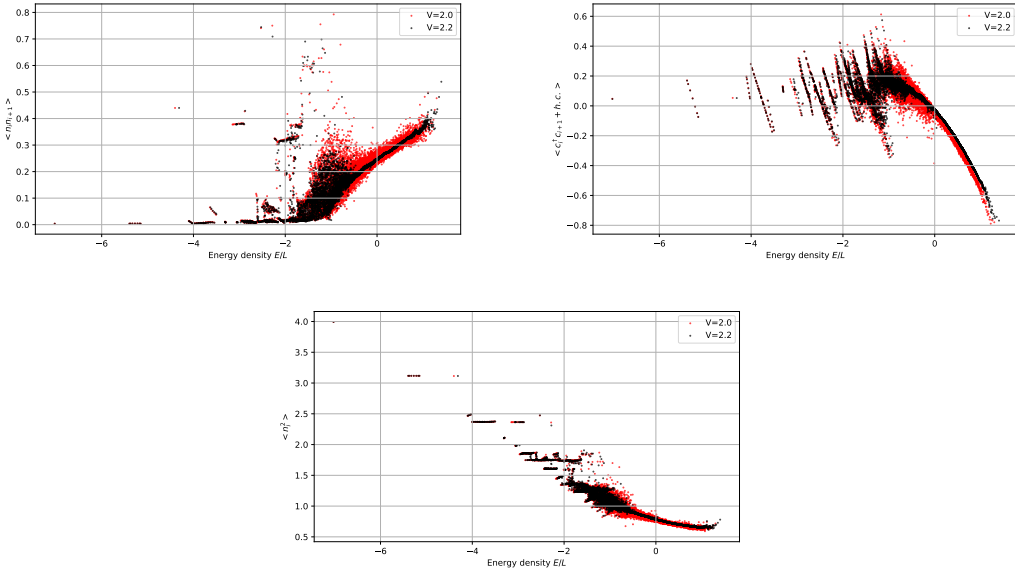


**Figure 3.9.** Eigenstate expectation value (EEV) plot for the eigenstates of with  $V = 2$  quenched to  $V = 2.2$ . We can see that the atypical states with energies near the edge of the continuum band are robust to the quench and retain their athermal nature. Other rare states with energy densities larger than -1 collapse to the continuum in the infinite time limit.

Again, we probe the short time out of equilibrium dynamics to investigate the relaxation behaviour of the atypical and typical states under a quench. We take the same random states as in (3.8.14) and (3.8.15) and evolve them in the Schrodinger picture by acting the unitary time evolution operator  $\hat{U} = e^{-i\hat{H}_f t/\hbar}$  on them producing:

$$|\psi_{typ}(t)\rangle = \sum_{i \in S_1} b_i e^{iH_f t} |E\rangle_i \quad (3.8.20)$$

$$|\psi_{atyp}(t)\rangle = \sum_{i \in S_2} c_i e^{iH_f t} |E\rangle_i \quad (3.8.21)$$

We evaluate the expectation value  $\langle n_i(t) n_{i+1}(t) \rangle$  in these two states:

We see that unlike under normal time evolution, the random states both relax to the same value when evolving under a quenched Hamiltonian. Consequently we have identified two different classes of atypical states. One type is robust to quenches, and can be found in the cluster at  $\frac{E}{L} \approx -1$ . These do seem to be rare in nature. The second type, with  $\frac{E}{L} \gtrsim -1$ , collapses to the continuum band in the infinite time limit, and exhibits signs relaxation at short and intermediate times. Due

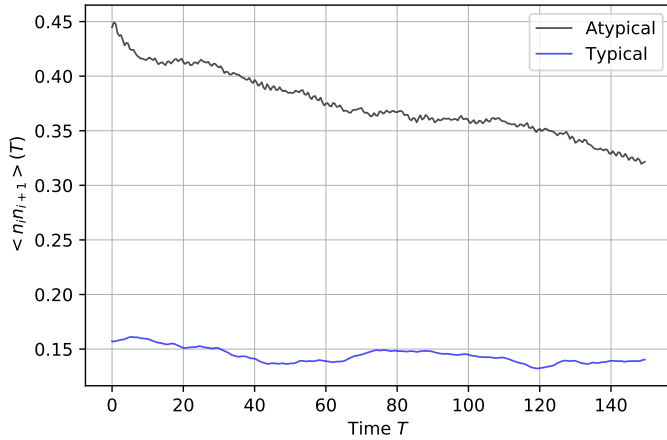


**Figure 3.10.** The expectation value  $\langle n_i n_{i+1} \rangle$  of (3.8.20) is plotted against time. We see that the atypical states starts relaxing towards the same value as the typical state even in the short time limit.

to this they may not be considered rare.

## 3.9 Two-chain model

### 3.9.1 The model and symmetries

We now consider the following EBHM on a two-chain system:

$$H = -t_x \sum_{i,j} (c_{i,j} c_{i+1,j} + h.c.) + \frac{U}{2} \sum_i n_i (n_i - 1) + V_x \sum_{i,j} n_{i,j} n_{i+1,j} + V_y \sum_{i,j} n_{i,j} n_{i,j+1} \quad (3.9.1)$$

where each chain has length  $L$ ,  $i = 0, 1, \dots, \frac{L}{2} - 1$  and  $j = 0, 1$  indexes the two chains. Also, we set the number of bosons to be  $N = L$ . We set PBCs along the chains, and OBCs between the chains. It follows that the model is translationally invariant along the chains, and has two parity symmetries corresponding to reflections in the perpendicular bisector of the chains and reflections swapping the two chains. We thus diagonalize in the  $k_x = 0, p_x = p_y = +1$  symmetry sector throughout this section.

### 3.9.2 Energy and EEV spacing statistics

We begin by looking at the spacing statistics. In fig. 3.11a we plot  $\mathcal{N}_{\Delta E}(E_i)$  for each energy level  $E_i$  (where  $E_i < E_{i+1}$  for all  $i$ ). The 4000th to 9000th eigenstates of (3.9.1) have approximately constant density of states, so this portion of the spectrum will be used to run the energy level and expectation value spacing statistics. Interestingly, the level spacing statistics do not follow a Wigner-Dyson distribution, signalling at possible integrability in our model. Nevertheless, this could be due to additional symmetries which we have not considered, and which would create degeneracies within the sector we are diagonalizing. It could also be that the system sizes under consideration are too small to produce an effectively non-integrable model. On the other hand, the off-diagonal elements appear to satisfy ETH, with far off-diagonal elements being very small,

and diagonal elements and close to diagonal elements being the largest. The vertical and horizontal lines which appeared in fig. 3.7a also appear here, but as we noted they are not indicative of any hidden structures preventing thermalization.

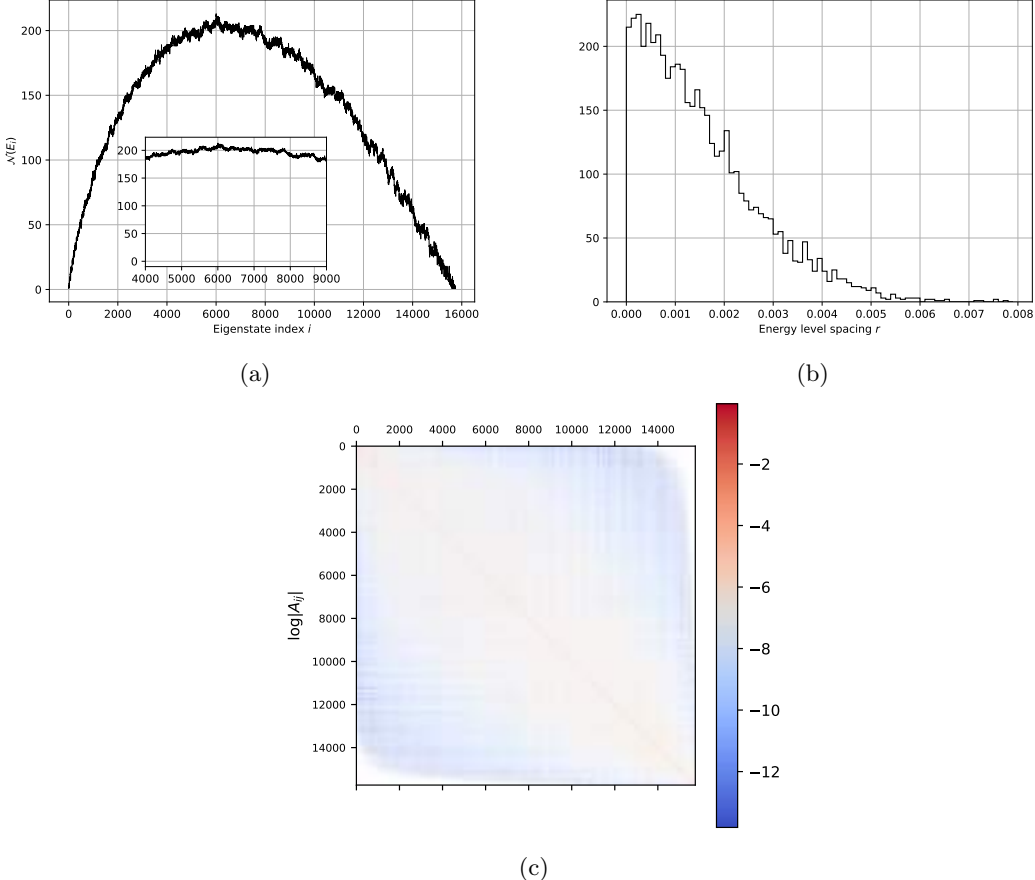


**Figure 3.11.** (a) Plot of  $\mathcal{N}_{\Delta E}(E_i)$ , the number of eigenstates with energy in the interval  $[E_i - \Delta/2, E_i + \Delta/2]$ , against the eigenstate index  $i$  (energy levels ordered in increasing energy) for  $L = 16$ . The inset shows the small variations in  $\mathcal{N}_{\Delta E}(E_i)$  (b) The energy level spacing distribution computed in the reduced spectrum plotted in the inset of ???. (c) The off diagonal elements of  $n_{i,j}n_{i+1,j}$  in the energy eigenbasis.

### 3.9.3 EEV plots

Next we map the EEV plots for  $n_{i,j}^2$ ,  $n_{i,j}n_{i+1,j}$  and  $n_{i,j}n_{i,j+1}$  averaged over the two chains since we are working in the  $k_x = 0, p_x = 0, p_y = 0$  block. It is important to distinguish even chain lengths  $\frac{L}{2}$  from odd chain lengths  $\frac{L}{2}$ . In the latter the periodic boundary conditions make it impossible to form a bipartite lattice, while in the former it is perfectly doable, as shown below in fig. 3.12.

Due to this distinction we plot the EEVs for even ( $L = 12, 16$ ) and odd ( $L = 10, 14$ ) length chains separately in the first two rows of fig. 3.13, while in the third row we compare  $L = 14$  and  $L = 16$ . We see that unlike the one-chain model, this two-chain model presents the formation of several bands which are most noticeable when looking at  $n_{i,j}n_{i+1,j}$  and  $n_{i,j}n_{i,j+1}$ . <sup>3</sup>.

<sup>3</sup>they are also present in  $n_{i,j}^2$  but are harder to see. It is easier to see the presence of bands by looking at the

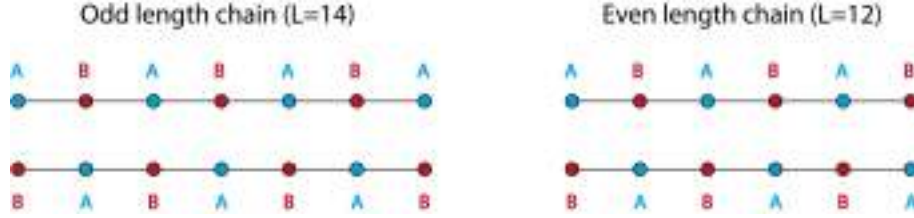
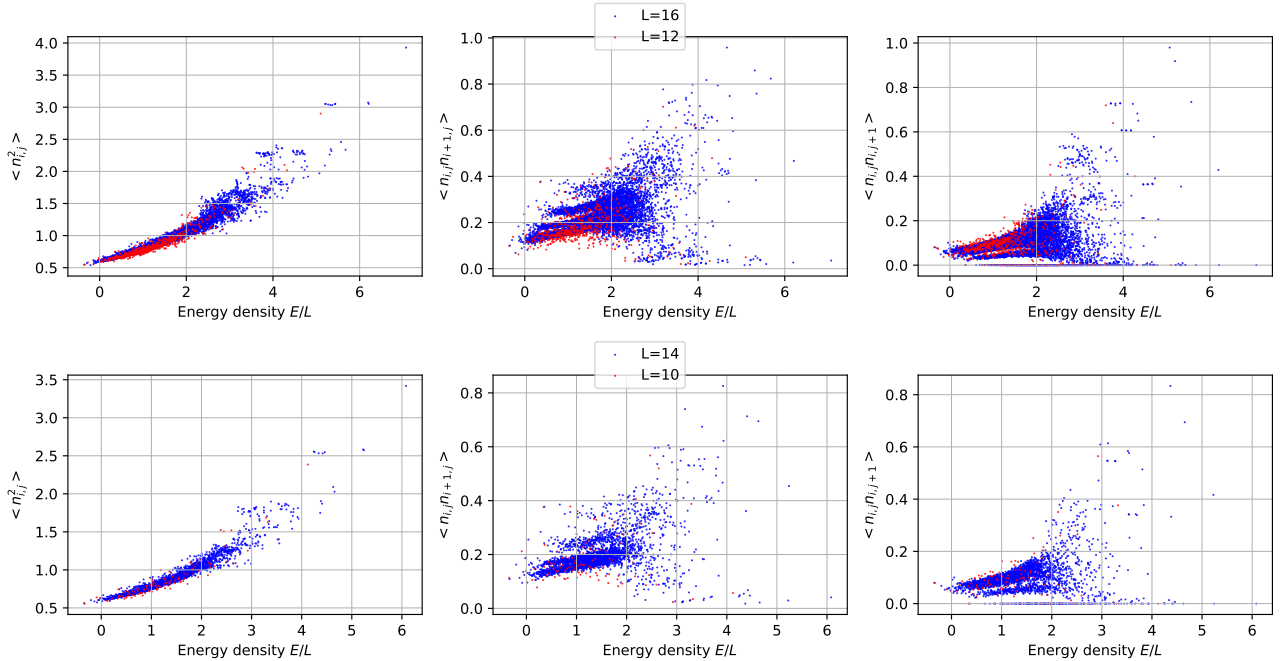


**Figure 3.12.** Formation of bipartite lattice in  $L = 14$  and  $L = 10$  shows that in the former case it is not possible to label each site with letters  $A$  or  $B$  without making at least two nearest neighbors have the same letter, while in the latter it can be done.

The features of these bands can be probed further by looking at the spacing between the expectation values of consecutive eigenstates (when ordered in increasing order of their respective energies). For an ergodic system it is easy to argue that this spacing should follow a gaussian which in the thermodynamic limit approaches a delta function due to the well-behavedness of expectation values as a function of energy. In our model we seem to notice an overall gaussian envelope with a major peak at zero spacing, but with several satellite peaks at larger spacings. We infer that each band should behave ergodically, but since we have several bands a small change in energy could lead to a jump in expectation value, thus violating ETH. To understand how the bands lead to these satellite peaks, consider an eigenstate whose EEV is in one of the bands shown above. As we slightly increase the energy the state can either remain in its original band, forming the central peak move to bands above/below it, forming the satellite peaks. In our case one can easily verify that the possible jumps between bands correspond to the peaks in the EEV spacing distribution, especially for  $\langle n_{i,j} n_{i,j+1} \rangle$  which has the most well formed bands.



EEV spacing plot.

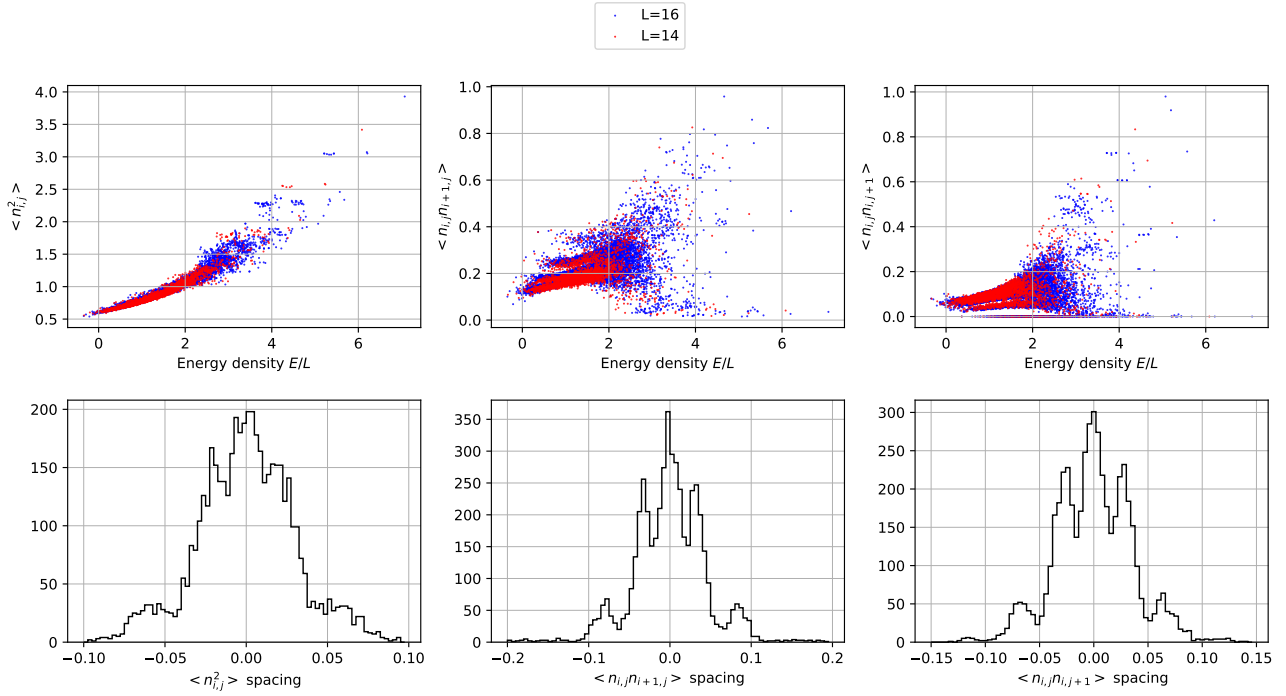


**Figure 3.13.** Plot of the EEVs for  $n_{i,j}^2$ ,  $n_{i,j}n_{i+1,j}$  and  $n_{i,j}n_{i,j+1}$  averaged over the two chains (which doesn't change anything due to the translational and parity invariance of (3.9.1)) for  $L = 12, 16$  (top row),  $L = 14, 10$  (second row),  $L = 16, 14$  (third row) and the corresponding expectation value spacing distribution for  $L = 16$  (bottom row).

### 3.9.4 Response to Quenches

The system is quenched following the same protocol as in the one-chain model, this time perturbing  $V_y$  suddenly from 2 to 2.2 at  $t = 0$ . The results are shown in fig. 3.14. Firstly, we again note that the quench helps in narrowing the bands, as was the case with the one chain model.

Furthermore, there are some states (colored in cyan in fig. 3.15) which are left unchanged by the quench, these are seen to correspond to the states with  $\langle n_{i,j}n_{i,j+1} \rangle = 0$  (which we refer to as “zero states”) when looking at the difference between the quenched and usual eigenstate expectation values. It follows that the zero states preserve their structure when mapping different expectation values. These zero states are atypical states robust to quenches in a strong way (they are exactly robust), while the robust atypical states in the one-chain model may be defined as robust to quenches only in a weak way (states close to each other in EEV remain close to each other).

## 3.10 Conclusions

ETH is an extremely powerful tool that allows one to conclude whether or not an isolated quantum system will reach thermal equilibrium. It states that thermalization can only occur for an observable if the expectation value of the associated quantum operator behaves as a smooth function of energy, and if the off diagonal matrix elements of this operator in the energy basis are sufficiently small. There are several known cases where ETH is broken strongly: a significant portion of the Hilbert

### 3.10. CONCLUSIONS

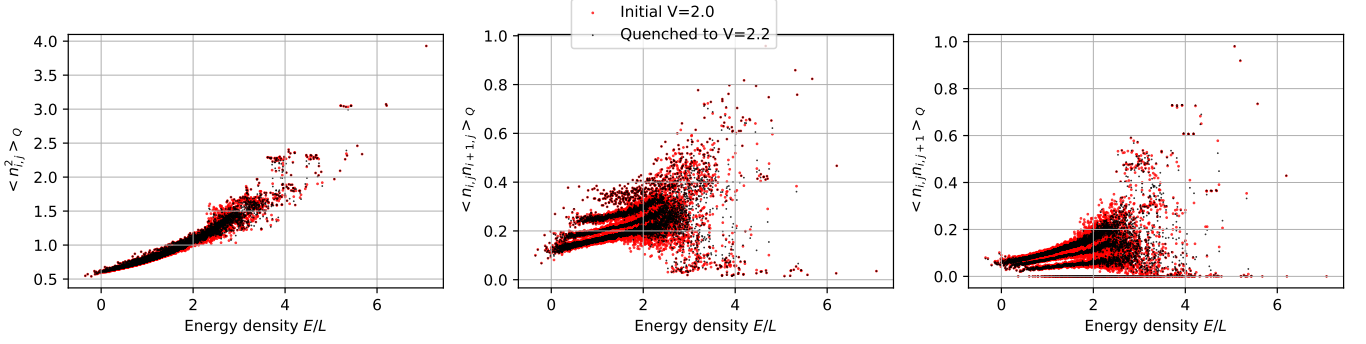


**Figure 3.14.** Plot of the typical EEVs for  $V=2.0$  in red and the corresponding quenched EEVs for  $V=2.2$  in red. The system size is  $L = 16$ .

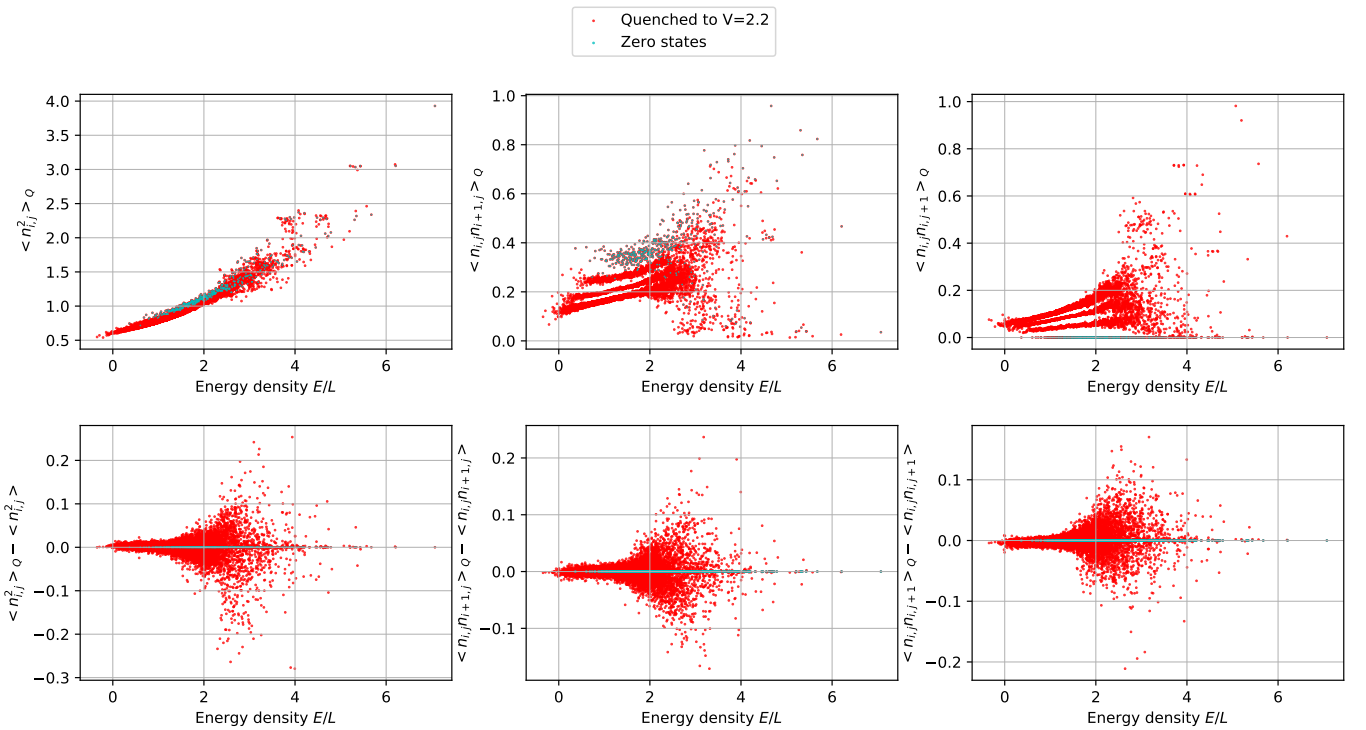


**Figure 3.15.** Top row: the quenched expectation values  $\langle A \rangle_Q$  (see (3.9)) are shown in red, with the ones that were left unchanged by the quench (which are the zero states) highlighted in cyan. Bottom row: the difference  $\langle A \rangle_Q - \langle A \rangle$  between the quenched and usual expectation values are shown in red, with the values corresponding to the unchanged states highlighted in cyan.

space avoids thermalization. On the other hand, ETH is known to apply to a plethora of chaotic systems. Recently, a lot of interest has been funneled into the study of systems mid-way between these two extreme, namely where only a vanishingly small part of the hilbert space violates ETH.

In this work, we thoroughly examined using exact diagonalization techniques two extended Bose-Hubbard models, one embedded on one chain with attractive onsite potential, and the other embedded on two chains with no hopping between them. We studied the level statistics of these hamiltonians and determined that our first model lacks integrability, while the other exhibits am-

biguous distributions which need further study, perhaps at larger system sizes. We then proceeded to examine the statement ETH makes on the diagonal matrix elements of our models. For the one chain model we noticed that while the majority of eigenstates formed a band that varied smoothly with energy, there were separate states, known as atypical, which were not well-behaved. The two-chain model exhibited atypical states in the form of several bands overlapping in energy. A system's dependence on its initial states is a hallmark of ergodicity breaking, and our models were confirmed to exhibit signs of this dependence when looking at EEV plots. An analysis of the matrix elements instead revealed that the off-diagonal elements were indeed exponentially suppressed and that this part of ETH was satisfied. We then turned our attention on the out of equilibrium dynamics of the atypical states which revealed that relaxation to the diagonal ensemble occured almost immediately, and that the athermality of our model could be probed at short times as well. We also examined the behaviour of the atypical states after a quench. This allowed us to categorize the atypical states into two classes, one which is robust to quenches and another which collapses into the well-behaved typical band in the infinite time limit. Furthermore, the robustness to quenches can be strong (the EEVs are left completely unchanged) and weak (the EEVs change but remain within the same band).

Future extensions of our work lie in the calculation of the entanglement entropy for the atypical states we identified. Due to the exponential scaling nature of the Hilbert space in our models, this is something that is currently numerically inaccessible. Another aspect that requires further investigation is the transition between lack and presence of thermalization at negative  $U$  and positive  $U$  respectively.

## Acknowledgments

I would like to thank my supervisors, Dr Andrew J.A. James and Dr. James P. Hague, for the immense support, guidance and the countless advice they have given me throughout the entirety of this project.

I would also like to thank the School of Physical Sciences for providing me with several resources, most importantly the computing cluster, without which most of the original work in this project would have been inaccessible.

---

# Bibliography

- [1] Dmitry A Abanin, Ehud Altman, Immanuel Bloch, and Maksym Serbyn. Colloquium: Many-body localization, thermalization, and entanglement. *Reviews of Modern Physics*, 91(2):021001, 2019.
- [2] Hannes Bernien, Sylvain Schwartz, Alexander Keesling, Harry Levine, Ahmed Omran, Hannes Pichler, Soonwon Choi, Alexander S Zibrov, Manuel Endres, Markus Greiner, et al. Probing many-body dynamics on a 51-atom quantum simulator. *Nature*, 551(7682):579–584, 2017.
- [3] Immanuel Bloch. Ultracold quantum gases in optical lattices. *Nature Physics*, 1(1):23–30, 2005.
- [4] Henrik Bruus and Karsten Flensberg. *Many-body quantum theory in condensed matter physics: an introduction*. OUP Oxford, 2004.
- [5] Luca D’Alessio, Yariv Kafri, Anatoli Polkovnikov, and Marcos Rigol. From quantum chaos and eigenstate thermalization to statistical mechanics and thermodynamics. *Advances in Physics*, 65(3):239–362, 2016.
- [6] J H de Boer and E J W Verwey. Semi-conductors with partially and with completely filled 3d-lattice bands. *Proceedings of the Physical Society (1926-1948)*, 49:59, 8 1937.
- [7] Josh M Deutsch. Quantum statistical mechanics in a closed system. *Physical review a*, 43(4):2046, 1991.
- [8] Joshua M Deutsch. Eigenstate thermalization hypothesis. *Reports on Progress in Physics*, 81(8):082001, 2018.
- [9] Freeman J Dyson. Statistical theory of the energy levels of complex systems. i. *Journal of Mathematical Physics*, 3(1):140–156, 1962.
- [10] Fabian H. L. Essler, Holger Frahm, Frank Göhmann, Andreas Klümper, and Vladimir E. Korepin. *The One-Dimensional Hubbard Model*. Cambridge University Press, 2005.
- [11] James R. Garrison and Tarun Grover. Does a single eigenstate encode the full hamiltonian? *Physical Review X*, 8(2), Apr 2018.
- [12] H. A. Gersch and G. C. Knollman. Quantum cell model for bosons. *Physical Review*, 129:959, 1 1963.
- [13] Markus Greiner, Olaf Mandel, Tilman Esslinger, Theodor W. Hänsch, and Immanuel Bloch. Quantum phase transition from a superfluid to a mott insulator in a gas of ultracold atoms. *Nature*, 415(6867):39–44, 2002.
- [14] Thomas Guhr, Axel MüllerGroeling, and Hans A. Weidenmüller. Random-matrix theories in quantum physics: common concepts. *Physics Reports*, 299(4):189–425, 1998.
- [15] JP Hague, S Downes, C MacCormick, and PE Kornilovitch. Cold rydberg atoms for quantum

---

## BIBLIOGRAPHY

---

- simulation of exotic condensed matter interactions. *Journal of Superconductivity and Novel Magnetism*, 27(4):937–940, 2014.
- [16] J. Hubbard. Electron correlations in narrow energy bands. *Proceedings of the Royal Society of London. Series A, Mathematical and Physical Sciences*, 276(1365):238–257, 1963.
  - [17] J. Hubbard. Electron correlations in narrow energy bands. ii. the degenerate band case. *Proceedings of the Royal Society of London. Series A, Mathematical and Physical Sciences*, 277(1369):237–259, 1964.
  - [18] J. Hubbard. Electron correlations in narrow energy bands. iii. an improved solution. *Proceedings of the Royal Society of London. Series A, Mathematical and Physical Sciences*, 281(1386):401–419, 1964.
  - [19] J. Hubbard. Electron correlations in narrow energy bands. iv. the atomic representation. *Proceedings of the Royal Society of London. Series A, Mathematical and Physical Sciences*, 285(1403):542–560, 1965.
  - [20] J. Hubbard. Electron correlations in narrow energy bands. v. a perturbation expansion about the atomic limit. *Proceedings of the Royal Society of London. Series A, Mathematical and Physical Sciences*, 296(1444):82–99, 1967.
  - [21] J. Hubbard. Electron correlations in narrow energy bands. vi. the connexion with many-body perturbation theory. *Proceedings of the Royal Society of London. Series A, Mathematical and Physical Sciences*, 296(1444):100–112, 1967.
  - [22] D. Jaksch, C. Bruder, J. I. Cirac, C. W. Gardiner, and P. Zoller. Cold bosonic atoms in optical lattices. *Physical Review Letters*, 81:3108–3111, 5 1998.
  - [23] D. Jaksch and P. Zoller. The cold atom hubbard toolbox. *Annals of Physics*, 315:52–79, 10 2004.
  - [24] Andrew JA James, Robert M Konik, and Neil J Robinson. Nonthermal states arising from confinement in one and two dimensions. *Physical review letters*, 122(13):130603, 2019.
  - [25] Robert Jördens, Niels Strohmaier, Kenneth Günter, Henning Moritz, and Tilman Esslinger. A mott insulator of fermionic atoms in an optical lattice. *Nature*, 455(7210):204–207, 2008.
  - [26] Hyungwon Kim, Tatsuhiko N. Ikeda, and David A. Huse. Testing whether all eigenstates obey the eigenstate thermalization hypothesis. *Phys. Rev. E*, 90:052105, Nov 2014.
  - [27] Corinna Kollath, Guillaume Roux, Giulio Biroli, and Andreas M Läuchli. Statistical properties of the spectrum of the extended bose–hubbard model. *Journal of Statistical Mechanics: Theory and Experiment*, 2010(08):P08011, aug 2010.
  - [28] Elliott H. Lieb and F. Y. Wu. Absence of mott transition in an exact solution of the short-range, one-band model in one dimension. *Physical Review Letters*, 20:1445, 6 1968.
  - [29] N. F. Mott. Metal-insulator transition. *Reviews of Modern Physics*, 40:677, 10 1968.
  - [30] Zlatko Papi. Weak ergodicity breaking through the lens of quantum entanglement, 2021.
  - [31] Marcos Rigol, Vanja Dunjko, and Maxim Olshanii. Thermalization and its mechanism for generic isolated quantum systems. *Nature*, 452(7189):854–858, 2008.
  - [32] Neil J Robinson, Andrew JA James, and Robert M Konik. Signatures of rare states and thermalization in a theory with confinement. *Physical Review B*, 99(19):195108, 2019.
  - [33] Anders W Sandvik. Computational studies of quantum spin systems. In *AIP Conference Proceedings*, volume 1297, pages 135–338. American Institute of Physics, 2010.

---

## BIBLIOGRAPHY

---

- [34] Naoto Shiraishi and Takashi Mori. Systematic construction of counterexamples to the eigenstate thermalization hypothesis. *Physical review letters*, 119(3):030601, 2017.
- [35] Mark Srednicki. Chaos and quantum thermalization. *Physical review e*, 50(2):888, 1994.
- [36] Mark Srednicki. Thermal fluctuations in quantized chaotic systems. *Journal of Physics A: Mathematical and General*, 29(4):L75L79, Feb 1996.
- [37] Mark Srednicki. The approach to thermal equilibrium in quantized chaotic systems. *Journal of Physics A: Mathematical and General*, 32(7):1163, 1999.
- [38] Christopher J Turner, Alexios A Michailidis, Dmitry A Abanin, Maksym Serbyn, and Zlatko Papić. Weak ergodicity breaking from quantum many-body scars. *Nature Physics*, 14(7):745–749, 2018.
- [39] Phillip Weinberg and Marin Bukov. QuSpin: a Python Package for Dynamics and Exact Diagonalisation of Quantum Many Body Systems part I: spin chains. *SciPost Phys.*, 2:003, 2017.
- [40] Phillip Weinberg and Marin Bukov. Quspin: a python package for dynamics and exact diagonalisation of quantum many body systems. part ii: bosons, fermions and higher spins. *SciPost Phys.*, 7(020):97, 2019.
- [41] Eugene P. Wigner. Characteristic vectors of bordered matrices with infinite dimensions. *Annals of Mathematics*, 62(3):548–564, 1955.
- [42] Eugene P Wigner. On the distribution of the roots of certain symmetric matrices. *Annals of Mathematics*, pages 325–327, 1958.
- [43] Eugene Paul Wigner. *Statistical properties of real symmetric matrices with many dimensions*. Princeton University, 1957.